Conformationally-Restricted Bicarbazoles with Phenylene Bridges Displaying Deep-Blue Emission and High Triplet Energies: Systematic Structure-Property Relationships

Iain A. Wright,*[a,b] Hameed A. Al-Attar,[c,d] Andrei S. Batsanov,[a] Andrew P. Monkman*[c] and Martin R. Bryce*[a]

[a] *Department of Chemistry, Durham University, South Road, Durham, DH1 3LE, UK*

[b] *Department of Chemistry, Loughborough University, Loughborough, Leicestershire, LE11 3TU, UK*

[c] *Department of Physics, Durham University, South Road, Durham, DH1 3LE, UK*

[d] *Department of Physics, Basrah University, Basrah, Iraq*

Abstract

The synthesis is reported of twelve new symmetrical carbazole dimers in which the carbazole units are linked via 1,4-phenylene spacers. There are two distinct series of compounds based on the position on the carbazole ring where the phenylene spacer is attached: this is either at carbazole C(3) (series **1a-1f**) or at C(2) (series **2a-2f**). The central phenylene ring is substituted with either two methyl, two methoxy or two cyano substituents which impart an intramolecular torsional angle between the phenylene and carbazole rings, thereby limiting the extent of π–conjugation between the carbazole units, and raising the triplet energies of the molecules to E_T 2.6 – 3.0 eV, as determined from their phosphorescence spectra at 80 K. Structure-property relationships were studied by UV-vis and fluorescence spectroscopy, cyclic voltammetry and theoretical calculations. A notable observation is that substitution at the 2-position of carbazole (linear conjugation) exerts control over the position of the HOMO, while substitution at the 3-position of carbazole (*meta* conjugation) allows greater control over the LUMO. X-ray crystal structures are reported for two of the bicarbazoles. Compound **2d** is shown to be a suitable host for the sky-blue emitter FIrpic in PhOLEDs, with improved device performance compared to CBP as host.

Introduction

Carbazole derivatives – small molecules,[1] linear oligomers,[2] dendrimers and star-shaped molecules,[3] and high molecular weight (co)polymers[4] – are ubiquitous π–conjugated systems in organic materials chemistry. They generally display high thermal, chemical and photochemical stability. The synthetic versatility of carbazole has led to derivatives that possess a range of outstanding optical and electronic properties, notably good hole-transporting ability, blue emission, high triplet energy levels and wide-band gaps, leading to their applications in organic light-emitting diodes (OLEDs), organic field-effect transistors, organic solar cells and sensors. There is, therefore, an ongoing quest for new and systematic variations in carbazole functionality to probe fundamental properties of relevance to practical organic electronics applications. Efficient synthetic pathways exist for functionalisation of carbazole at the nitrogen atom and at the C(2) or C(3) positions. Difunctionalisation at the 2,7 or 3,6-positions is also generally straightforward, whereas substitution at the 1 or 1,8-positions is unusual.

In this context, bicarbazole derivatives are appealing targets. For example, they are well established host molecules for triplet-state green and blue guest emitters in OLEDs. A prerequisite for their application as hosts is that their triplet energy (E_T) must be higher than that of the emitting guest. A classic example is 4,4'-bis(9-carbazolyl)-2,2'-biphenyl (CBP) (Figure 1). It has a triplet energy of ca. 2.6 eV, which is sufficiently high to host green phosphors as dopants, but not high enough to prevent reverse energy transfer from a blue-emitting guest back to the host.[5] A structurally modified molecule, 1,3-bis(9-carbazolyl)-benzene (mCP), with a higher E_T of ca. 3.00 eV is a host in phosphorescent sky-blue and blue OLEDs, for example using the dopant emitter bis[(4',6'-difluorophenyl)pyridinato-*N*,*C*2']iridium(III) picolinate (FIrpic).[6]

There is, therefore, considerable interest in optimising the optoelectronic properties, especially the triplet level, of new bicarbazole derivatives. Recent studies which report molecules with E_T raised to ca. 2.9 eV include CBP analogues with *meta*-linkage of the carbazole units to the central biphenyl unit;[7] *para*-linked CBP analogues with sterically-locked carbazole–4,4'-biphenyl junctions,[8] and the incorporation of a 2,2'-dimethylbiphenyl core between the carbazoles.[9] In the above examples both carbazole units are linked to the core by *N*-substitution. Representative modifications involving C–C linked bicarbazoles include 3,3'-bicarbazoles with tailored substituents on nitrogen,[10,11,12] related 3,4' and 4,4'-bicarbazoles,[11] and bicarbazoles with conjugated alkenyl and alkynyl spacers connected at the 1-, 2- and 3-positions of the carbazole units.[13]

We now report twelve symmetrical carbazole dimers in which the carbazole units are linked via a series of 1,4-phenylene spacers. The dimers comprise two distinct series based on the connectivity at the carbazole ring: this is either at C(3) (series **1a-1f**) or at C(2) of carbazole (series **2a-2f**) (Figure 1), the latter potentially giving more extended *para*-phenylene conjugation throughout the molecules. In each case the central phenylene ring bears either two methyl, two methoxy or two cyano substituents. These substituents are designed to serve two purposes: (i) to tune the optoelectronic properties by electron-withdrawing or electron-donating effects, and (ii) more significantly, to impart a substantial intramolecular torsional angle between the phenylene and carbazole rings which will limit the extent of conjugation between the carbazole units, thereby raising the triplet energies of the molecules. We present the thermal, optical and electrochemical properties of the molecules. Additional information about their structural properties was obtained from single-crystal X-ray diffraction data of two of the compounds and from density functional theory (DFT) calculations.

Results and Discussion

Synthesis

Suzuki cross-coupling protocols were employed to synthesise the bicarbazole derivatives. Suitably substituted phenylenediboronic acid pinacol ester bridge units **A**,[14] **B**[15] and **C**,[16] were reacted with the corresponding bromocarbazole derivatives **3**,[17] **4**,[17] **5** [18] and **6** (Figure 1).[19] A two-fold Suzuki coupling approach was used initially for the synthesis of **1a** with conventional heating, $Pd(OAc)_2$/SPhos catalyst and with K_3PO_4 as a base. It was subsequently found to be more expedient to use microwave-assisted synthesis according to the procedure of Lindoy *et al*.[20] which greatly reduced reaction times and gave comparable yields to the conventional approach. Synthetic details are reported in the Supporting Information.

Yields of the products were typically ca. 30-40% and were restricted by the limited solubility of the target structures and intermediates thereof, alongside competing homocoupling or hydrolysis of the boronate esters.[13] Purification of some of the bicarbazole products was unexpectedly challenging and was ultimately achieved by a combination of column chromatography and repeated recrystallisation. During chromatography the materials had a tendency to stick to the stationary phase of the column making the endpoint of bands difficult to identify using typical thin layer chromatography (TLC). Traces of the desired compounds were clearly evident on the TLC plate long after the bulk of the material had eluted. As a general observation, the *N*-phenyl analogues **1d-f** and **2d-f** were easier to purify than *N*-ethyl analogues **1a-c** and **2a-c**, particularly by recrystallisation. Crystals of **1d-f** and **2d-f** grew slowly as polycrystalline solids, whereas **1a-c** and **2a-c** were difficult to dissolve in common organic solvents and then tended to precipitate as amorphous powders. In *N*-phenylcarbazole the bulky pendant phenyl group sits out of plane with the carbazole,[21] which may help to disrupt intermolecular π-stacking interactions between carbazoles to a greater extent than the smaller *N*-ethyl moiety, facilitating a more controlled crystallisation. However, crystalline samples of these molecules could be obtained by making a dilute solution in hot EtOAc prior to addition of hexane until the cloud point was reached followed by slow cooling. If necessary, the solutions were then stored in a fridge until the crystallisation was complete. The target compounds were unambiguously characterised by ^{1}H and ^{13}C NMR spectroscopy, high resolution mass spectrometry and, in most cases, elemental analysis. The identity of **1a** and **1c** was further confirmed by single crystal X-ray analysis.

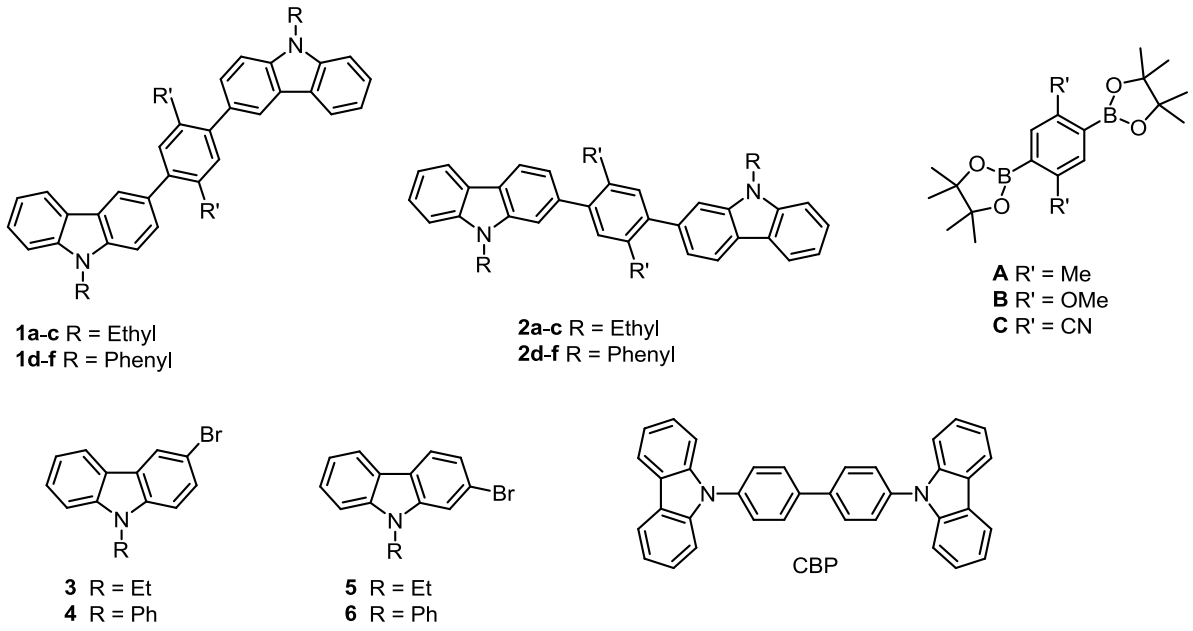

Figure 1. Structures of the bicarbazole derivatives **1a-f** and **2a-f** synthesised in this work, and their precursors **A-C** and **3-6**. CBP is included as a reference compound.

Table 1. Bicarbazole derivatives synthesised in this work.

	R	R'	Yield / %
1a	Et	Me	45
1b	Et	OMe	43
1c	Et	CN	35
1d	Ph	Me	31
1e	Ph	OMe	48
1f	Ph	CN	33
2a	Et	Me	30
2b	Et	OMe	31
2c	Et	CN	18
2d	Ph	Me	41
2e	Ph	OMe	46
2f	Ph	CN	40

Structural and thermal properties

Single crystals, suitable for X-ray analysis were obtained for compounds **1a** and **1c**. The structures are shown in Figure 2. Molecule **1a** has a crystallographic inversion centre; the methyl group is disordered between two alternative positions with occupancies of 82 and 18%. The carbazole moiety is planar and forms a dihedral angle (τ) of 51.0° with the central phenylene ring. The crystal of **1c** contains two crystallographically non-equivalent molecules, both lying at inversion centres and twisted similarly to **1a**, with τ = 49.1° and 45.9°.

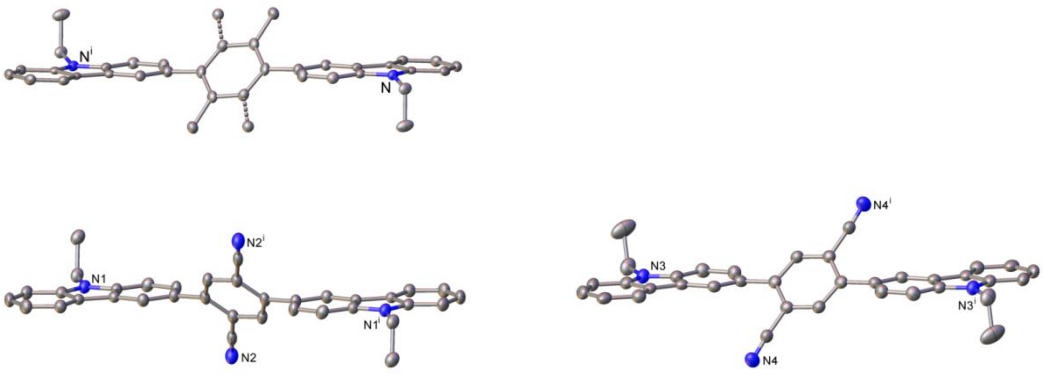

Figure 2. Molecular structures of **1a** (top) showing the major (82%, solid) and minor (18%, dashed) methyl positions, and (bottom) two symmetrically independent molecules of **1c**. Primed atoms are generated by inversion centres. All H atoms are omitted for clarity.

To investigate the thermal properties of the bicarbazole derivatives, differential scanning calorimetry (DSC) measurements were performed. These data confirm that the compounds **1a-1f** and **2a-2f** have high glass transition temperatures (T_g) in the range of 130 – 150 °C and they all remain amorphous upon cooling. These values are consistent with previous rigid bicarbazole systems,[8] and T_g of > 100 °C combined with a stable amorphous phase is advantageous for operational stability in OLEDs.[8a]

Photophysics

The absorption and photoluminescence (PL) properties of the compounds were measured as drop-cast thin films in Zeonex host. The normalised absorbance spectra for **1a-1f** and **2a-2f** are shown in Figures S1 and S2 in ESI and the data are listed in Table 2, along with CBP as a model compound. The optical band gaps, calculated from the onset of the absorption spectra, are given in Table 2. The absorption spectral profiles show the expected features of carbazole derivatives with strong bands at high energy assigned to optically allowed π–π* transitions.[8b,13a] The room temperature emission spectra for **1a-1f** and **2a-2f** are shown in Figures 3a and 3b. The PL spectra can be grouped into three zones, marked on Figure 3, according to the two methyl, methoxy or cyano substituents on the central phenylene ring. The spectra are systematically red shifted in the order Me (zone A) < OMe (zone B) < CN (zone C) giving emission ranging from deep blue (A) to blue-green (C). These trends are discussed below.

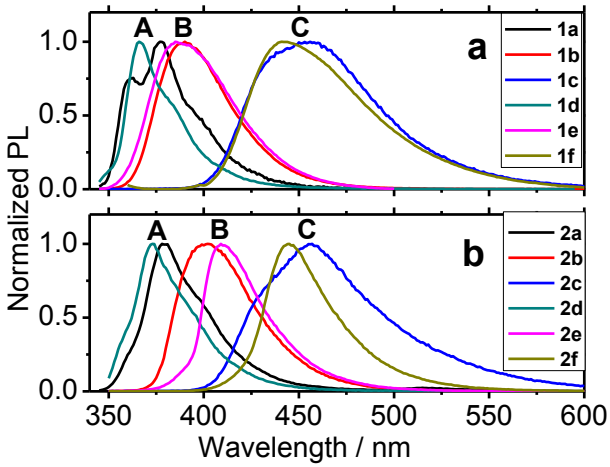

Fig. 3. Normalised photoluminescence spectra for the bicarbazole derivatives. a) **1a-1f** and b) **2a-2f** as drop-cast thin films in Zeonex host, 1:50 w/w ratio at room temperature. The notation **A**, **B** and **C** above the spectra refer to zones based on the central substituents: Me (zone A); OMe (zone B); CN (zone C).

The main focus of the photophysical study was, however, to determine the triplet energies of the compounds from their phosphorescence spectra recorded at 80 K (Figure 4). The triplet energies calculated from the peak and onset values are listed in Table 2.

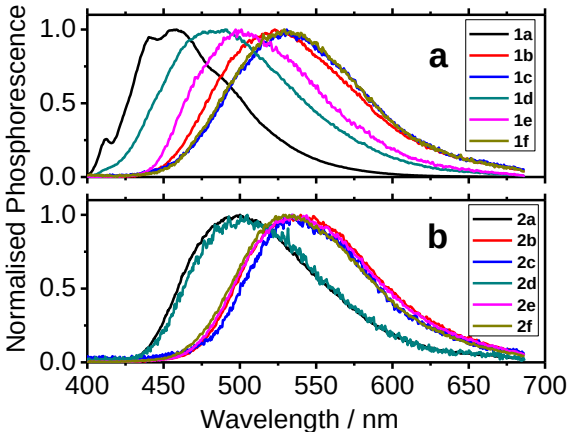

Figure 4. Normalised phosphorescence spectra for the bicarbazole derivatives a) **1a-1f** and b) **2a-2f** as drop-cast thin films in Zeonex host, 1:50 w/w ratio at 80 K.

The photophysical data for the highest triplet energy bicarbazole derivative **1a** compared with CBP in zeonex are shown in Figure 5. For CBP the absorption features associated with transitions localised on the carbazole are identified at 340 nm and 290 nm. These two bands are also observable in **1a.** An additional broader absorption centred at about 322 nm is observed for CBP, but not for **1a**. This feature is likely to be associated with transitions between orbitals that involve the central biphenyl unit of CBP.[8b] In the fluorescence spectra, in contrast, CBP and **1a** show very similar vibrational structures with maxima at ca. 360 nm and 378 nm for both compounds. The phosphorescence spectrum of **1a**, however, shows a large blue shift compared with CBP and the analogues **1b-f** and **2a-f**. This is ascribed to the reduced conjugation within this molecule compared to the other compounds reported herein (see the computational study below).

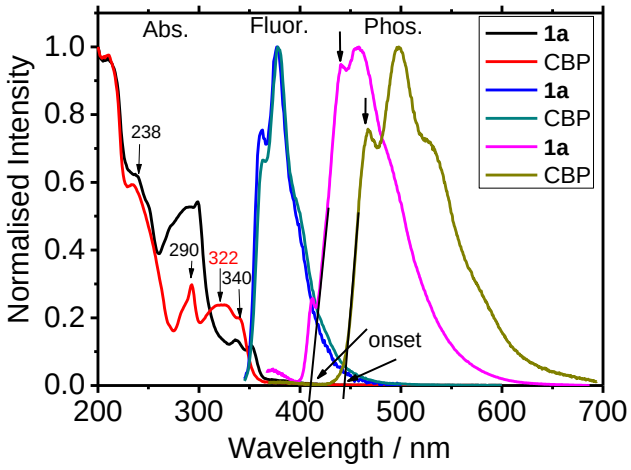

Figure 5. Absorption (Abs.), Fluorescence (Fluor.) and Phosphorecence (Phos.) of bicarbazole derivative **1a** compared with CBP in Zeonex matrix. The arrows on the phosphorescence spectra mark the onset and peak positions used to obtain the triplet energies stated in Table 2.

Table 2. Photophysical and electrochemical data of bicarbazole derivatives.

	λ_{Abs} (nm)[a]	$\lambda_{Abs(onset)}$ (nm)[a]	E_g (eV)[a]	$\lambda_{max(PL)}$ (nm)[a]	PLQY (%)[a,b]	$\lambda_{(phos.)}$ Onset, Peak (nm)[a]	E_T Onset, Peak (eV)[c]	E_{ox} vs F_c^+/F_c (V)[d]	E_{HOMO} (eV)[e]	E_{LUMO} (eV)[e]
CBP	236, 292 322, 340, 348	354	3.50	365, 376	57	460, 478	2.69, 2.59	0.80[f,g]	-5.90[i]	-2.40[i]
1a	240, 299, 336, 352	365	3.39	362, 377	27	416, 470	2.98, 2.63	0.63[g]	-5.72	-2.33
1b	238, 288, 301, 324	368	3.37	390	38	450, 523	2.70, 2.37	0.41,[h] 0.58[h]	-5.51	-2.14
1c	238, 297, 393	446	2.78	454	19	462, 529	2.68, 2.34	0.81[g]	-5.91	-3.13
1d	296, 332, 346	355	3.49	371	12	420, 480	2.90, 2.58	0.70[g]	-5.80	-2.31
1e	243, 299, 324	378	3.28	385	60	443, 500	2.85, 2.46	0.50,[h] 0.67[h]	-5.62	-2.34
1f	242, 296, 387	432	2.87	440	49	457, 528	2.71, 2.35	0.83[g]	-5.93	-3.06
2a	237, 265,	359	3.45	379	26	439, 498	2.80, 2.50	0.72[g]	-5.82	-2.37

	309									
2b	237, 263, 340	384	3.24	402	41	474, 536	2.60, 2.31	0.57,[h] 0.77[h]	-5.67	-2.43
2c	234, 265, 320, 376	427	2.90	456	28	474, 534	2.60, 2.32	0.75[g]	-5.85	-2.95
2d	263, 294, 313	357	3.47	372	29	433, 500	2.86, 2.48	0.79[g]	-5.88	-2.41
2e	239, 257, 294, 343	386	3.21	410	42	469, 534	2.64, 2.32	0.74,[h] 0.90[h]	-5.84	-2.63
2f	240, 260, 320, 372	417	2.97	444	37	467, 530	2.65, 2.34	0.91[g]	-6.01	-3.04

[a] All optical data were collected from a drop cast film in Zeonex (1:50 w/w).
[b] Estimated error ±10%.
[c] Phosphorescent emission were collected at 80 K from drop cast films in Zeonex (1:50 w/w), YAG laser pulses at 352 nm, delay 40 ms, gate 10 ms.
[d] CV data were obtained from solutions of 1 mmol of the compound, 0.1 M *n*-Bu_4NBF_4 in CH_2Cl_2, scan rate 100 mV/s, using a platinum disc working electrode, a silver wire reference electrode and a platinum wire counter electrode. E_{ox} is the onset of the first oxidation wave. Potentials are given versus F_c^+/F_c couple used as internal reference.
[e] E_{HOMO} = -($E_{onset,ox}$ vs F_c^+/F_c + vacuum level) eV. Vacuum level taken as 5.10 eV.[22] $E_{LUMO} = E_{HOMO}+E_g$ (E_g, Abs_{onset}). For compound **1e** (Figure 6) as a representative: E_{HOMO} = -(1.15 - 0.65 + 5.10) = -5.60 eV; E_{LUMO} = -5.60 + 3.28 = -2.32 eV.
[f] A value of E_{ox} = 0.87 V vs Fc^+/Fc in DCM was obtained for CBP by differential pulse voltammetry in reference 8b.
[g] Irreversible wave.
[h] Reversible wave.
[i] Values of -5.97 and -2.45 eV were obtained for E_{HOMO} and E_{LUMO}, respectively in reference 8b.

The general trends in the photophysical data are as follows:

a) Varying the substituent on nitrogen (9-ethyl or 9-phenyl) has only a minimal effect on the optical properties, with no significant differences between the series of compounds.

b) Series **2a-f** generally have red-shifted emission, consistent with extended conjugation through the five *para*-linked phenylene rings in **2a-f**, compared to only the central three *para*-linked phenylene rings of series **1a-f**.

c) The substituents on the central phenylene ring result in a consistent red-shift in emission in the order Me < OMe < CN. This trend can be explained by conjugative effects within the π–system. The broadened and red-shifted PL spectra of the dicyano derivatives **1c**, **1f**, **2c** and **2f** (Figure 3, zone C) are consistent with intramolecular charge transfer from donor carbazole to the electron-withdrawing dicyanophenylene core. The dimethoxy substituents in the core of **1b**, **1e**, **2b** and **2e** extend the conjugation and hence red shift the emission (Figure 3, zone B) and do not show vibronic structure compared to the non-conjugating dimethylphenylene analogues **1a**, **1d**, **2a** and **2d** (Figure 3, zone A).

d) With the exception of **1e** (Φ_{PL} 60%), the new derivatives (**1b-f** and **2a-f**) all have lower PLQY values (Φ_{PL} 12-49%) than CBP (Φ_{PL} 57%) in Zeonex film (1:50 w/w). This may indicate that the reduced rigidity of **1a-f** and **2a-f** increases thermal vibrational quenching which reduces the PLQY. A marked lowering of PLQY compared to CBP was observed by Gantenbein et al. in solution studies of CBP analogues with locked carbazole-biphenyl junctions and the reduction was ascribed to enhanced triplet yields.[8b]

e) The new bicarbazole derivatives all show phosphorescence emission at 80 K with broader spectra compared to CBP. Triplet energies for series **1a-f** are in the range E_T 2.98-2.68 (peak onset) and 2.63-2.34 eV (peak maximum), and series **2a-f** are in the range 2.86-2.60 (peak onset) and 2.50-2.31 eV

(peak maximum). Notably, **1a** (2.98, 2.63 eV) and **1d** (2.90, 2.58 eV) show the highest triplet energies of the new derivatives. For comparison CBP has E_T 2.69, 2.59 eV for peak onset and maximum, respectively, measured under identical conditions. Compound **2d** (2.86, 2.48 eV) is shown to be a suitable host for the sky-blue emitter FIrpic in PhOLEDs, with improved device performance compared to CBP as host (see below).

Electrochemistry

The solution electrochemical properties of the compounds were studied by cyclic voltammetry (CV) to determine their electron donating ability. The HOMO levels were estimated from the onset potential of the first oxidation relative to ferrocene. None of the compounds showed a reduction process within the accessible solvent window scanning to -2.00 V. Therefore, the LUMO levels were deduced by adding the optical band gap to the HOMO levels. The limitations of using this standard protocol to obtain LUMO levels are well recognised.[22b] The oxidation potentials are listed in Table 2 and are related to the oxidation of the carbazolyl groups, as suggested from the distribution of the HOMO orbitals (see below). The following general structure/property trends are observed in the CV data.

a) Reversibility: The derivatives with methoxy substituents on the bridge (**1b**, **1e**, **2b** and **2e**) are the most easily oxidised and show two reversible waves, whereas for the Me and CN substituted bridges the waves are irreversible. Representative CVs are shown for compound **1e** in Figure 6 and for **1a** in Figure S8 of ESI. The irreversibility is ascribed to the dimerisation of the radical cationic species at the 3,6-positions of carbazole.[8,13a,23] The separation of the two 1-electron oxidation waves for some of our bicarbazoles is consistent with previous work on carbazole dimers with conjugated acetylenic or olefinic spacers.[13a] The separation is observed for those derivatives with the lowest oxidation potentials – notably **1b** and **1e**. In general, the NEt compounds also demonstrate a stronger tendancy to adsorb onto the electrode surface as evidenced by the presence of cathodic stripping peaks upon reversal of polarity, and/or the growth of new bands in the voltammogram which increase in magnitude upon repeated cycling.

b) Oxidation potentials: The oxidation potentials are anodically shifted depending on the bridge substituents in the sequence E_{ox} OMe < Me < CN. For specific data compare **1b**(OMe) 0.41 V < **1a**(Me) 0.63 V < **1c**(CN) 0.81 V, or **2e**(OMe) 0.74 V < **2d**(Me) 0.79 V < **2f**(CN) 0.91 V.

c) Effect of the substituent on nitrogen: NPh versus NEt. For the same bridge, in all cases the NPh derivative has a higher oxidation potential compared to the NEt analogue. The shift is, however, rather variable and is between a minimum of 20 mV (compare **1c** and **1f**) and a maximum of 170 mV (compare **2b** and **2e**).

d) Connectivity at carbazole C(3) (series **1a-1f**) versus C(2) (series **2a-2f**): The oxidation potential of series **1** derivatives is generally lower than for series **2** isomers. We can attribute this to the fact that the HOMO of series **1** contains a higher bridge contribution than that of series **2** where the HOMO is localised over the carbazole. The carbazole C(3) is *para* to the delocalised lone pair of the ring nitrogen which facilitates increased delocalisation over the bridge. This effect will be much weaker across C(2) and ultimately gives the HOMO of the C(3) series a longer effective conjugation length,

and therefore lower oxidation potential, than the C(2) series despite having an overall shorter linear conjugation length. A similar trend was observed for conjugated acetylenic or olefinic spacers[13a] and is also borne out in our computational analysis in the following section. The only exception is the oxidation potentials of **1c** (E_{ox} 0.81 V) / **2c** (E_{ox} 0.75 V).

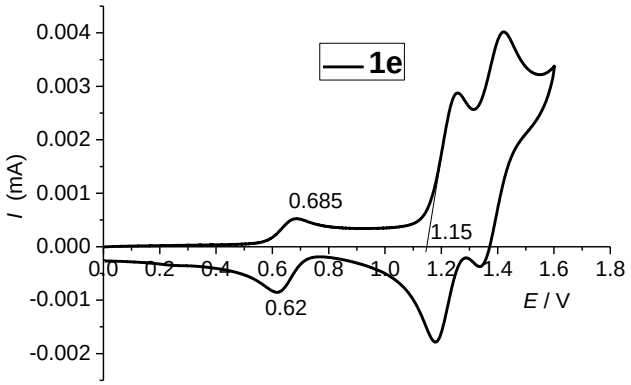

Figure 6. CV scan of compound **1e** with internal ferrocene reference centered at 0.65 V. The electrochemical cell comprised a platinum disc working electrode, a silver wire reference electrode and a platinum wire counter electrode. Data were recorded at room temperature using 1.0 mM concentration of **1e** and 0.1 M solution of *n*-Bu_4NBF_4 in dichloromethane at a scan rate of 100 mV s^{-1}.

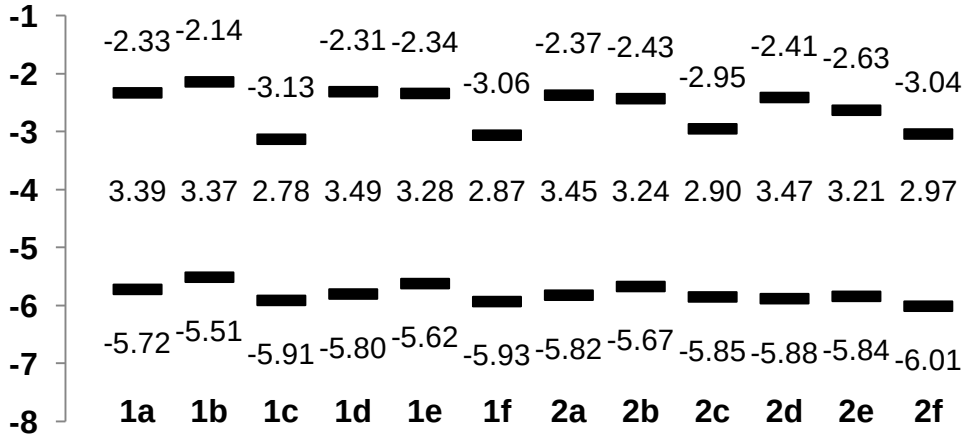

Figure 7. Experimentally-determined HOMO-LUMO energy levels (eV) of compounds **1** and **2**.

DFT and Frontier Molecular Orbital Study

Density function theory (DFT) calculations were performed with ORCA v3.03[24] using the B3LYP hybrid functional and 6-31G* basis set.[25] Ground state structural optimisations were performed prior to frontier orbital calculations. Molecular orbital plots for the HOMO and LUMO of **1a-f** and **2a-f** are shown in Figures 8 and 9, respectively, along with the unsubstituted *p*-phenylene bridged analogue**s7-10** for comparison. The calculated HOMO-LUMO gaps are summarised in Table S1. Plots of the other frontier orbitals are shown in Figures S3-S6 in ESI.

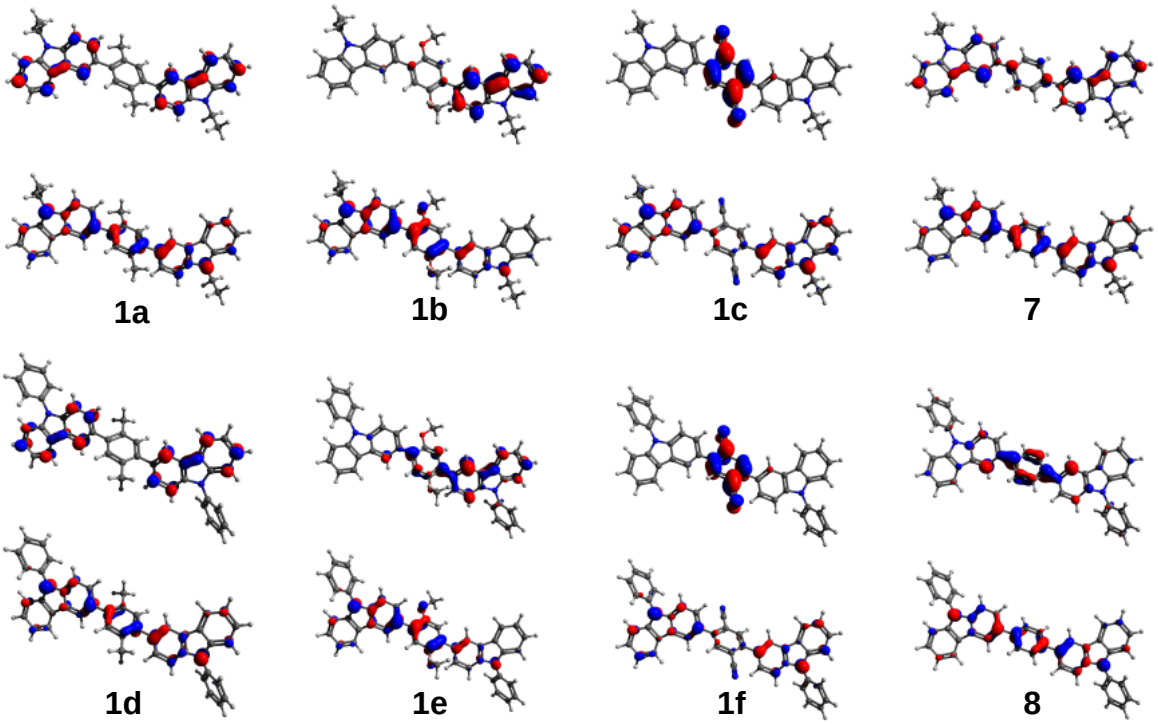

Figure 8 Molecular orbital plots for the 3-carbazole derivatives **1a-f** alongside the *p*-phenylene bridged analogues **7** and **8** obtained from DFT (B3LYP/6-31G*). For each structure HOMO is lower and LUMO is upper diagram.

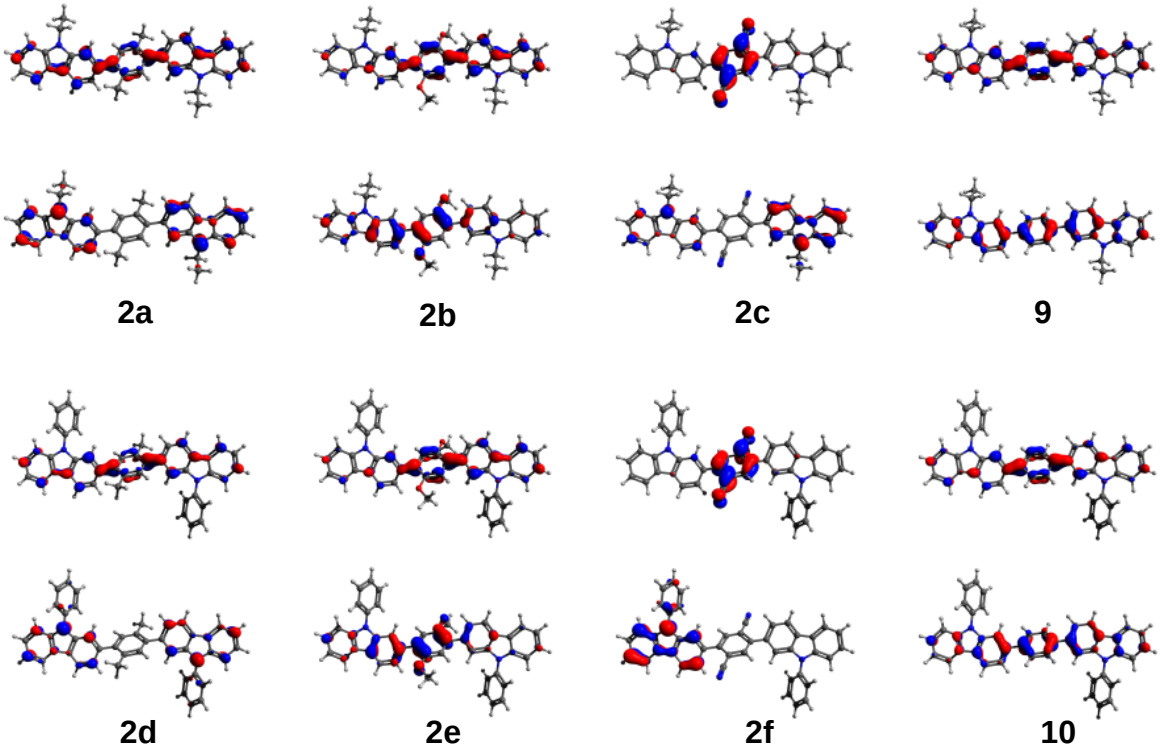

Figure 9 Molecular orbital plots for the 2-carbazole derivatives **2a-f** and the *p*-phenylene bridged analogues **9** and **10**

obtained from DFT (B3LYP/6-31G*). For each structure HOMO is the lower and LUMO is the upper diagram.

The following general trends are apparent:

1) Compounds **1a**,**d** and **2a**,**d** with methyl substituents on the bridging phenylene ring show the largest dihedral angles between the bridge and carbazole, typically with $\tau = 53°$. (The calculated dihedral angle for all compounds can be found in Table S2 in ESI). These compounds also consistently have the largest HOMO-LUMO gap within both series due to a combination of the disruption in linear conjugation imposed by the steric bulk of methyl substituents and their limited electronic influence as weak donors. These observations are verified experimentally in both the electrochemistry and optical spectroscopy.
2) In compounds **1b**,**e** and **2b**,**e** the bridge has two strongly electron donating methoxy substituents and, consequently, the HOMO is predominantly localised on the bridge with a lesser contribution from one of the two adjacent carbazoles. The influence of this can be seen in the electrochemical behaviour of these molecules as any electrochemically generated radical cations or dications will remain more localised over the bridge at the centre of the molecule. This will hinder them from reacting with other molecules in solution and helps to explain the improved electrochemical reversibility of these molecules when compared to the other members of the series, and the presence of two separated redox waves (Table 2 and Figure 6).

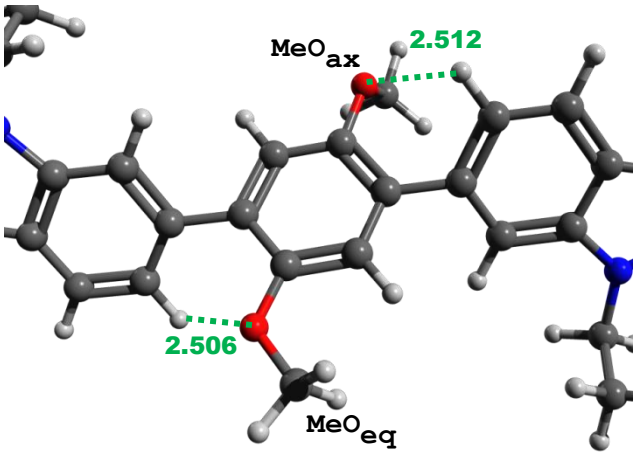

Figure 10 Intramolecular O•••H interactions on the calculated structure of **2b**. This example is representative of the other members of the series with a dimethoxy bridge **1b**,**e** and **2e**.

3) There is an asymmetry to the distribution of the HOMO for **1b**,**e** and **2b**,**e** which is not seen for the other members of the series. This is attributed to non-covalent H•••O interactions between the oxygen of one MeO- group and the hydrogen atom of an adjacent carbazole (Figure 10). One methoxy group (MeO_{ax}) sits axially with respect to the central phenyl ring while the other assumes an equatorial geometry (MeO_{eq}). The interatomic O•••H distances vary between 2.486 and 2.512 Å across the series, as shown in Table S2, and this interaction has a planarising influence on the molecule resulting in $\tau = 42–47°$. The interatomic distances are within typical hydrogen bonding range.[26] The electron rich nature of the dimethoxy bridge coupled with this planarising influence results in an increase in the

HOMO and reduction in the LUMO energy level when compared to the methyl containing homologues (**1a**,**d** and **2a**,**d**). This is borne out experimentally by the red-shift in absorption and emission behaviour for the methoxy derivatives and in their electrochemical measurements.

4) For the four dicyanophenylene bridged compounds **1c**,**f** and **2c**,**f** the LUMO is localised exclusively on the electron poor bridge and is much lower in energy while the HOMO manifold contains minimal contribution from the bridge. The intramolecular charge transfer behaviour of these molecules is clearly apparent in the UV/vis absorption spectra. When compared to the dimethyl analogues these molecules also demonstrate increased planarity between adjacent rings with $\tau = 44-46°$.
5) The presence of the bridge at the 2-carbazole position results in increased degeneracy of the HOMO manifold (Figure S7, ESI). We attribute this to the longer linear conjugation lengths of **2a-f** which results in more balanced contributions from the carbazole rings and the bridge. This also results in the LUMO being delocalised in a quinoidal fashion over the bridge and adjacent carbazole rings which lowers the energy of the LUMO overall with respect to **1a-f**. This will planarise the excited state, as has been observed in alkyne-bridged analogues.[13a] Conversely, the bridge at the 3-carbazole position in **1a**,**b** and **2a**,**b** increases the degeneracy of the LUMO manifold. This is not observed in **1c** and **2c** due to the much more strongly electron withdrawing dicyanophenylene bridge dominating the LUMO.
6) The calculated E_g for *N*-phenyl is marginally wider than for *N*-ethyl analogues in some instances and the HOMO and LUMO for *N*-phenyl both tend to sit slightly lower in energy. This indicates some additional stabilisation is achieved by the presence of the *N*-phenyl ring and is verified experimentally, with the exception of **2c** and **2f**. The reason for these exceptions is not obvious.

As compounds **1a**,**d** and **2a**,**d** have shown the most desirable optical properties, calculations were also performed on the analogous compounds **7**-**10** featuring a non-substituted *p*-phenylene bridge to obtain a deeper insight into the influence of the sterically incumbent methyl substituents. Compound **7** has been synthesised previously and used in OLEDs.[27] The optical and computational data of the *N*-octyl analogue of **9** have been reported and they agree with the present data.[28] In particular, the authors note that the fluorescence spectra of this molecule in solution is sharp with clear substructure indicating a more planarised excited state which agrees with our DFT results. The dihedral angle between carbazole and the *p*-phenylene bridge for the compounds **7**-**10** is $\tau = 36-37°$ in all cases. Therefore, it is clear that by incorporating methyl substituents on the phenylene bridge in **1a,d** and **2a,d** τ has increased significantly. This limits the extent of electronic communication along the chain, resulting in a significant widening of the HOMO-LUMO gap. This is consistent with the experimental data.

PhOLED characterisation

PhOLEDs were fabricated using derivative **2d** as the host. For this study **2d** was chosen from within the series of new bicarbazoles because of its high triplet energy (Table 2) and relative ease of synthesis and purification. To confirm that the high triplet derivative **2d** was suitable as a host material in PhOLEDs, FIrpic was chosen as the archetypal sky-blue emitter.[6] Directly comparable devices were fabricated using **2d** and CBP as the host. The device structure was: ITO/ NBP (40 nm)/TAPC(10 nm)/18% FIrpic in CBP or in **2d** host(35 nm)/ TAZ(10 nm)/ TPBi(40 nm)/ LiF(0.8 nm)/ Al (100 nm), with all the layers deposited by thermal evaporation

under vacuum. NBP = *N*,*N*′-di(1-naphthyl)-*N*,*N*′-diphenyl-(1,1′-biphenyl)-4,4′-diamine; TAPC = (1,1-bis{4-*N*,*N*-di(*p*-tolyl)amino]phenyl}cyclohexane); FIrpic = iridium(III) bis[4,6-(di-fluorophenyl)pyridinato-*N*,*C*2′]picolinate; TAZ = 3-(biphenyl-4-yl)-5-(4-*tert*-butylphenyl)-4-phenyl-4*H*-1,2,4-triazole; TPBi = 2,2′,2″-(1,3,5-benzenetriyl)tris-[1-phenyl-1*H*-benzimidazole]. The EL spectrum of both devices is identical, with emission exclusively from the dopant FIrpic (Fig. 11). Both **2d** and CBP devices exhibit very similar *J*-*V* characteristics (Fig. 11b). Demonstrating that both devices have similar electron and hole injection and transport through the multilayer structure. Thus, the superior performance of the device with **2d** is ascribed to the improved exciton confinement and reduced exciton quenching due to the higher triplet energy of the **2d** host. Fig. 11c shows the external quantum efficiency (EQE) and Fig. 11d shows the device current efficiency (DevE) versus brightness. For the **2d**-host device the EQE and DevE at 200 cd/m^2 are 12.7 % and 30 cd/A, respectively. At 1000 cd/m^2 the values are 8.7% and 19.5 cd/A respectively. For the CBP-host device, the efficiencies at 200 cd/m^2 and at 1000 cd/m^2 are 7% and 6% for EQE, and 15.7 cd/A and 14 cd/A for DevE, respectively.

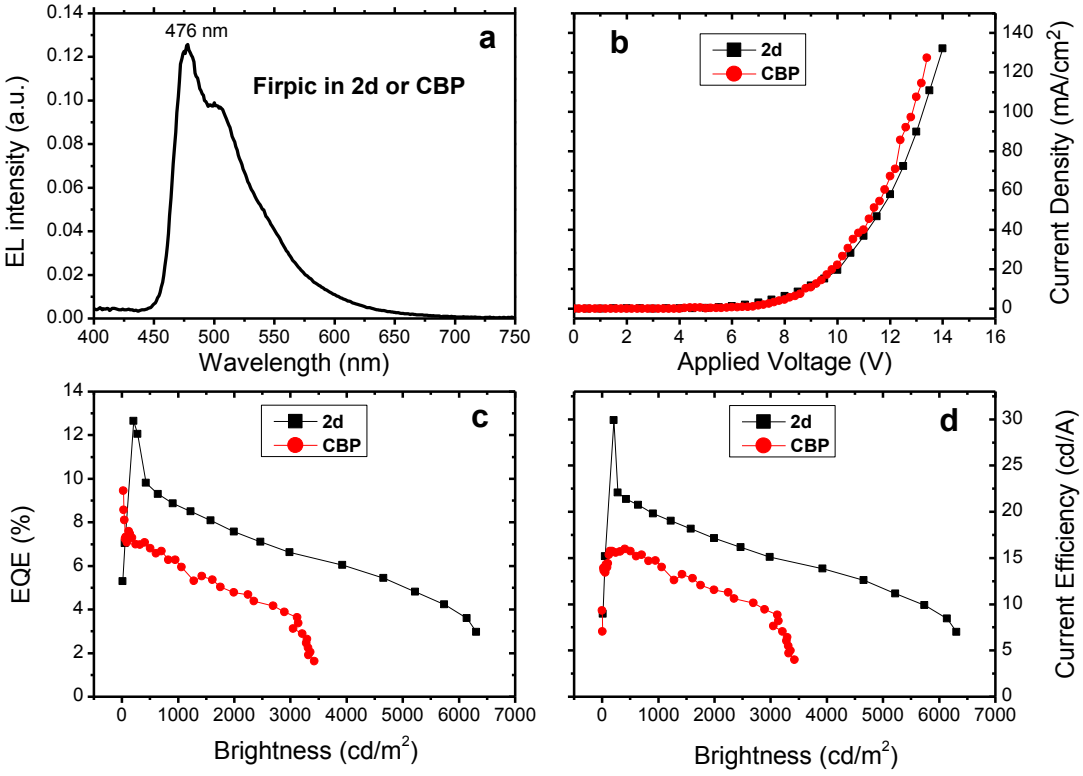

Figure 11 a) EL spectrum for devices with **2d** or CBP as host, showing emission exclusively from FIrpic dopant. b) *J*-*V* characteristics. c) External quantum efficiency. d) Device current efficiency.

Conclusions.

The new bicarbazole derivatives **1a-f** and **2a-f** have been rationally designed and synthesised by two-fold Suzuki cross-coupling reactions, and their optoelectronic and structural properties have been characterized. A particular focus was on assessing the effect of functionalisation of carbazole at C(3) (series **1a-1f**) or at C(2) (series **2a-2f**) on the fine-tuning of the physical properties of the molecules. The introduction of a 2,5-disubstituted 1,4-phenylene bridge in the conjugated backbone provides a desirable blue shift in

emission. This is due to the twist induced by the sterically demanding substituents which increases the HOMO-LUMO gap. A further notable observation is that substitution at the 2-position of carbazole (linear conjugation) exerts control over the position of the HOMO, while substitution at the 3-position of carbazole (*meta* conjugation) allows greater control over the LUMO. This increased degeneracy in the HOMO or LUMO manifold with respect to conjugation length holds for both *N*-ethyl and *N*-phenyl carbazoles and is also maintained when the non-substituted 1,4-phenylene bridge is employed. While some electronic delocalisation along the conjugated backbone must be maintained the use of bulkier, branched secondary alkyls in place of methyl substituents may provide further widening of the HOMO-LUMO gap which presents an accessible route to materials suitable for hosting blue or deep-blue organometallic phosphors or as deep-blue fluorophores in their own right.

Acknowledgements.
The authors acknowledge the financial support of EPSRC grant EP/K016164/1. IAW would like to thank Loughborough University for startup funding.

Supporting Information Available: Synthesis and characterisation of bicarbazole derivatives, copies of NMR spectra and thermal analysis data; X-ray crystallographic data for **1a** and **1c**; additional photophysical electrochemical and computational data; PhOLED data.

1 (a) P-I. Shih, C-L. Chiang, A. K. Dixit, C.-K. Chen, M-C. Yuan, R-Y. Lee, C-T. Chen, E. W-G. Diau and C-F. Shu, *Org. Lett.*, 2006, **8**, 2799–2802; (b) K. R. J. Thomas, J. T. Lin, Y.-T. Tao and C.-W. Ko, *J. Am. Chem. Soc.*, 2001, **123**, 9404−9411; (c) A. L. Fisher, K. E. Linton, K. T. Kamtekar, C. Pearson, M. R. Bryce and M. C. Petty, *Chem. Mater*., 2011, **23**, 1640–1642; (d) Q. Zhang, J. Li, K. Shizu, S. Huang, S. Hirata, H. Miyazaki, and C. Adachi, *J. Am. Chem. Soc.*, 2012, **134**, 14706–14709; (e) F. B. Dias, K. N. Bourdakos, V. Jankus, K. C. Moss, K. T. Kamtekar, V. Bhalla, J. Santos, M. R. Bryce and A. P. Monkman, *Adv. Mater*., 2013, **25**, 3707–3714; (f) D. Zhang, M. Cai, Y. Zhang, Z. Bin, D. Zhang and L. Duan, *ACS Appl. Mater. Interfaces*, 2016, **8**, 3825−3832. (g) K. Guo, H. Wang, Z. Wang, C. Si, C. Peng, G. Chen, J. Zhang, G. Wang and B. Wei, *Chem. Sci.*, 2017, **8**, 1259–1268.

2 (a) M.-H. Tsai, Y.-H. Hong, C.-H. Chang, H.-C. Su, C.-C. Wu, A. Matoliukstyte, J. Simokaitiene, S. Grigalevicius, J. V. Grazulevicius and C.-P. Hsu, *Adv. Mater*., 2007, **19**, 862–866; (b) M. Sonntag and P. Strohriegl, *Chem. Mater.*, 2004, **16**, 4736–4742; (c) N. Drolet, Morin, J.-F., N. Leclerc, S. Wakim, Y. Tao and M. Leclerc, *Adv. Funct. Mater*., 2005, **15**, 1671–1682. (d) Z. Zhao, X. Xu, H. Wang, P. Lu, G. Yu and Y. Liu, *J. Org. Chem*., 2008, **73**, 594–602; (e) S. U. Pandya, H. A. Al-Attar, V. Jankus, Y. Zheng, M. R. Bryce and A. P. Monkman, *J. Mater. Chem*., 2011, **21,** 18439–18446.

3 (a) I. Hwang, U. Selig, S. S. Y. Chen, P. E. Shaw, T. Brixner, P. L. Burn and G. D. Scholes, *J. Phys. Chem. A*, 2013, **117**, 6270–6278. (b) K. Albrecht, K. Matsuoka, K. Fujita and Y. Yamamoto, *Angew. Chem. Int. Ed.*, 2015, **54**, 5677–5682. (c) T. Keawin, N. Prachumrak, S. Namuangruk, S. Pansay, N. Kungwan, S. Maensiri, S. Jungsuttiwong, T. Sudyoadsuk and V. Promarak, *RSC Adv*., 2015, **5**, 73481–73489. (d) N. A. Kukhta, D. Volyniuk, J. V. Grazulevicius and G. Juska, *J. Phys. Chem. C* 2016, **120**, 1208–1217.

4 (a) J. V. Grazulevicius, P. Strohriegl, J. Pielichowski and K. Pielichowski, *Prog. Polym. Sci*., 2003, **28**, 1297–1353. (b) S. Beaupre, P. L. T. Boudrealt and M. Leclerc, *Adv. Mater*., 2010, **22**, E6–E27; (c) F. Dumur, *Org. Elect.*, 2015, **25**, 345–361; (c) J. H. Cook, J. Santos, H. A. Al-Attar, M. R. Bryce and A. P. Monkman, *J. Mater. Chem. C*, 2015, **3**, 9664–9669; (d) A. van Dijken, J. J. A. M. Bastiaansen, N. M. M. Kiggen, B. M. W. Langerveld, C. Rothe, A. Monkman, I. Bach, P. Stossel and K. Brunner, *J. Am. Chem. Soc*., 2004, **126**, 7718–7727; (e) Y. Geng, M. A. Ali, A. J. Clulow, S. Fan, P. L. Burn, I. R. Gentle, P. Meredith and P. E. Shaw, *Nature Commun*., 2015, **6**, Art No. 8240; (f) T. Wang, A. J. Pearson, A. D. F. Dunbar, P. A. Staniec, D. C. Watters, H. Yi, A. J. Ryan, R. A. L. Jones, A. Iraqi and D. G. Lidzey, *Adv. Funct. Mater*., 2012, **22**, 1399–1408.

5 C. Adachi, R. C. Kwong, P. Djurovich, V. Adamovich, M. A. Baldo, M. E. Thompson and S. R. Forrest, *Appl. Phys. Lett.*, 2001, **79**, 2082.

6 (a) R. J. Holmes, S. R. Forrest, Y.-J. Tung, R. C. Kwong, J. J. Brown, S. Garon and M. E. Thompson, *Appl. Phys. Lett.*, 2003, **82**, 2422; (b) E. Baranoff and F. B. Curchod, *Dalton Trans.*, **2015**, *44*, 8318–8329.

7 (a) P. Schrogel, N. Langer, C. Schildknecht, G. Wagenblast, C. Lennartz and P. Strohriegl, *Org. Elect.*, 2011, **12**, 2047–2055; (b) S. A. Bagnich, A. Rudnick, P. Schroegel, P. Strohriegl and A. Köhler, *Phil. Trans. R. Soc. A*, 2015, **373**, 20140446.

8 (a) P. Schrogel, A. Tomkeviciene, P. Strohriegl, S. T. Hoffmann, A. Kohler and C. Lennartz, *J. Mater. Chem*., 2011, **21**, 2266–2273; (b) M. Gantenbein, M. Hellstern, L. Le Pleux, M. Neuburger and M. Mayor, *Chem. Mater*., 2015, **27**, 1772–1779.

9 I. Tanaka, Y. Tabata and S Tokito, *Chem. Phys. Lett*., 2004, **400**, 86–89.

10 X. Cao, J. Hu, Y. Tao, H. Yuan, J. Jin, X. Ma, X. Zhang and W. Huang, *Dyes and Pigments*, 2017, **136**, 543–552.

11 M. Kim and J. Y. Lee, *ACS Appl. Mater. Interfaces*, 2014, **6**, 14874-14880.

12 H. Sasabe, N. Toyota, H. Nakanishi, T. Ishizaka, Y. Pu and J. Kido, *Adv. Mater*., 2012, **24**, 3212–3217.

13 (a) S. Kato, H. Noguchi, A. Kobayashi, T. Yoshihara, S. Tobita and Y. Nakamura, *J. Org. Chem*., 2012, **77**, 9120−9133; (b) C.-H. Chen, J. T. Lin and M.-C. P. Yea, *Tetrahedron*, 2006, **62**, 8564–8570. (c) Y. Song, C. Di, Z. Wei, T. Zhao, W. Xu, Y. Liu, D. Zhang and D. Zhu, *Chem.Eur. J*., 2008, **14**, 4731–4740.

14 S. Grunder, C. Valente, A. C. Whalley, S. Sampath, J. Portmann, Y. Y. Botros, and J. F. Stoddart, *Chem. Eur. J*., 2012, **18**, 15632–15649.

15 J. A. Kerszulis, C. M. Amb, A. L. Dyer, and J. R. Reynolds, *Macromolecules*, 2014, **47**, 5462–5469.

16 G. A. Chotana, M. A. Rak, and M. R. Smith III, *J. Am. Chem. Soc.*, 2005,**127**, 10539–10544.

17 S. H. Kim, I. Cho, M. K. Sim, S. Park, and S. Y. Park, *J. Mater. Chem.*, 2011, **21**, 9139–9148.

18 C. J. Kelley, K. Ansu, W. Budisusetyo, A. Ghiorghis, Y. Qin, and J. M. Kauffman, *J. Heterocyclic Chem.*, 2001, **38**, 11–23.

19 A. Keerthi and S. Valiyaveettil, *J. Phys. Chem. B*, 2012, **116**, 4603–4614.

20 C. R. K. Glasson, G. V. Meehan, C. A. Motti, J. K. Clegg, P. Turner, P. Jensen, and L. F. Lindoy, *Dalton Trans.*, 2011, **40**, 10481–10490.

21 (a) V.A. Galievsky, S.I. Druzhinin, A. Demeter, P. Mayer, S.A. Kovalenko, T.A. Senyushkina and K. A. Zachariasse, *J. Phys. Chem. A*, 2010, **114**, 12622–12638. (b) C. Avendaño, M. Espada, B. Ocaña, S.

García-Granda, M. del Rosario Díaz, B. Tejerina, F. Gómez-Beltrán, A. Martinez and J. Elguero, *J. Chem. Soc., Perkin Trans. 2,* 1993, 1547–1555.

22. (a) C. M. Cardona, W. Li, A. E. Kaifer, D. Stockdale and G. C. Bazan, *Adv. Mater*., 2011, **23**, 2367–2371; (b) J-L. Bredas, *Mater. Horiz*., 2014, **1**, 17–19.

23. J.-F. Morin, M. Leclerc, D. Adès and A. Siove, *Macromol. Rapid Commun.,* 2005, **26**, 761–778.

24. F. Neese, *WIREs Comput. Mol. Sci.*, 2012, **2**, 73–78.

25. (a) W. J. Hehre, R. Ditchfield and J. A. Pople, *J. Chem. Phys.*, 1972, **56**, 2257–2261; (b) J. D. Dill and J. A. Pople, *J. Chem. Phys.*, 1975, **62**, 2921–2923; (c) M. M. Francl, W. J. Pietro, W. J. Hehre, J. S. Binkley, M. S. Gordon, D. J. DeFrees and J. A. Pople, *J. Chem. Phys.*, 1982, **77**, 3654–3665; (d) V. A. Rassolov, J. A. Pople, M. A. Ratner and T. L. Windus, *J. Chem. Phys.*, 1998, **109**, 1223–1229.

26. G. R. Desiraju, *Angew. Chem. Int. Ed*., 2011, **50**, 52–59.

27. G. Kruciate, R. Griniene, A. Tomkeviciene, J. V. Grazulevicius, L. Liu, B. Zhang, Z. Xie and S. Grigalevicius, *Optical Materials,* 2013, **36**, 444−448.

28. M. Belletête, M. Bédard, J. Bouchard, M. Leclerc and G. Durocher, *Can. J. Chem.*, 2004, **82**, 1280–1288.

Supporting Information

Conformationally-Restricted Bicarbazoles with Phenylene Bridges Displaying Deep-Blue Emission and High Triplet Energies: Systematic Structure-Property Relationships

Iain A. Wright,*[a,b] Hameed A. Al-Attar,[c,d] Andrei S. Batsanov,[a] Andrew P. Monkman*[c] and Martin R. Bryce*[a]

[a] *Department of Chemistry, Durham University, South Road, Durham, DH1 3LE, UK*

[b] *Department of Chemistry, Loughborough University, Loughborough, Leicestershire, LE11 3TU, UK*

[c] *Department of Physics, Durham University, South Road, Durham, DH1 3LE, UK*

[d] *Department of Physics, Basrah University, Basrah, Iraq*

General information

All commercially available chemicals were used without further purification. Reactions requiring an inert atmosphere were performed under a blanket of argon gas, which was dried over a phosphorus pentoxide column. Anhydrous solvents were dried through an HPLC column on an Innovative Technology Inc. solvent-purification system. Column chromatography was performed using 40–60 μm mesh silica gel. Analytical thin-layer chromatography (TLC) was performed on plates precoated with silica gel (Merck, silica gel 60F254) and visualized using UV light (254, 315, 365 nm). NMR spectra were recorded on Bruker Avance 400 MHz and Varian Mercury 400 MHz spectrometers. Melting points were determined in open-ended capillaries using a Stuart Scientific SMP3 melting point apparatus at a ramping rate of 1 °C/min. Atmospheric solids analysis probe (ASAP) mass spectra were recorded on a Waters Xevo QTOF spectrometer. Elemental analyses were obtained on an Exeter Analytical Inc. CE-440 elemental analyser. Differential scanning calorimetry (DSC) was performed in a nitrogen atmosphere using a Mettler Toledo DSC 3 instrument. The compounds were heated at a rate of 10 ^{o}C /min. UV-Vis and photoluminescence spectra for all samples were obtained using Shimadzu UV-3600 and Jobin Yvon Luminescence spectrometers (FluoroMax-3). For cyclic voltammetry measurements the electrochemical cell comprised a platinum disc working electrode, a silver wire reference electrode and a platinum wire counter electrode. Data were recorded at room temperature using 1.0 mM concentrations of all compounds in 0.1 M solutions of *n*-Bu_4NBF_4, 99% (Sigma Aldrich) in dichloromethane (CH_2Cl_2), CHROMASOLV®, 99.9% (Sigma Aldrich) at a scan

rate of 100 mV s^{-1} and were calibrated against a ferrocene/ferrocenium redox couple as internal standard.

Synthetic details

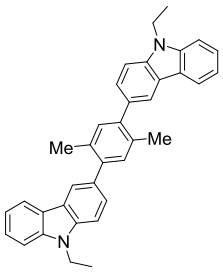

1a

Under an atmosphere of Ar, 3-bromo-9-ethylcarbazole **3** (150 mg, 0.55 mmol), bridge **A** (90 mg, 0.25 mmol), $Pd(OAc)_2$ (1 mg, 2 %) and SPhos (4 mg, 4%) were dissolved in degassed toluene (10 mL) prior to addition of an aqueous K_3PO_4 (2.7 M, 1.6 mL, 4.4 mmol) and heated to reflux for 20 h. Upon cooling the reaction mixture was diluted with EtOAc (25 mL) and washed with water (25 mL) then dried over $MgSO_4$ prior to removal of solvent under reduced pressure and evaporation of solvent under reduced pressure. Purification was achieved by column chromatography (10% EtOAc/hexane) followed by recrystallization from EtOAc/hexane to yield the product as a white crystalline solid (56 mg, 45%). mp. 222-224°C

^{1}H-NMR (400 MHz, DMSO-d_6): δ = 8.23 (d, J = 7.5 Hz, 2H), 8.19 (d, J = 1.6 Hz, 2H), 7.68 (d, J = 8.4 Hz, 2H), 7.64 (d, J = 8.2 Hz, 2H), 7.50 (dd, J = 8.4, 1.6 Hz, 2H), 7.48 (ddd, J = 8.3, 7.2, 1.2 Hz, 2H), 7.27 (s, 2H), 7.24 – 7.18 (m, 2H), 4.50 (q, J = 7.2 Hz, 4H), 2.33 (s, 6H), 1.37 (t, J = 7.1 Hz, 6H)

^{13}C-NMR (101 MHz, DMSO-d_6): δ = 140.6, 139.9, 138.5, 132.2, 132.1, 131.9, 126.9, 125.8, 122.23, 122.16, 120.7, 120.6, 118.7, 109.1, 108.7, 37.0, 20.0, 13.8

MS ($ASAP^+$): m/z = 493.2 [$M+H^+$]

HRMS ($ASAP^+$): m/z = calculated for $C_{36}H_{33}N_2$ [$M+H^+$]: 493.2644; found: 493.2642

Elemental analysis: Found C, 87.58; H, 6.58; N, 5.49 Calculated C, 87.77; H, 6.55; N, 5.69

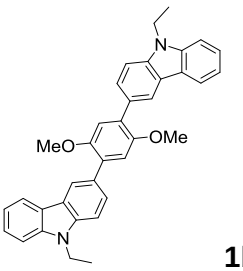

1b

Under argon, bridge **B** (117 mg, 0.30 mmol) and **3** (186 mg, 0.68 mmol) were added to a microwave vial containing $Pd(PPh_3)_4$ (25 mg, 0.02 mmol) and K_2CO_3 (300 mg, 2.17 mmol) and suspended in a degassed mixture of DMF (3 mL) and H_2O (1 mL) before the vial was sealed. The vial was then heated at 120 °C in a microwave reactor for 25 minutes. Upon cooling, the tube was opened and the reaction mixture poured into water and filtered. The solids thus obtained were then dissolved in dichloromethane and dried over $MgSO_4$ prior to removal of solvent under reduced pressure.

Purification was achieved by column chromatography (10% THF/hexane) followed by recrystallisation from toluene/methanol to give **1b** as a white crystalline powder (68 mg, 43%). mp. 247-249 °C (blackens)

N.B. Addition of a few drops of CS_2 to the NMR sample was required to inhibit aggregation and obtain well-resolved NMR spectra.

^{1}H-NMR (400 MHz, DMSO-d_6): δ = 8.30 (d, *J* = 1.7 Hz, 2H), 8.16 (d, *J* = 7.5 Hz, 2H), 7.70 (dd, *J* = 8.5, 1.7 Hz, 2H), 7.61 (d, *J* = 8.9 Hz, 2H), 7.58 (d, *J* = 8.4 Hz, 2H), 7.46 (ddd, *J* = 8.3, 7.1, 1.2 Hz, 2H), 7.21 (ddd, *J* = 7.9, 7.1, 1.0 Hz, 2H), 7.14 (s, 2H), 4.50 (q, *J* = 7.1 Hz, 4H), 3.83 (s, 6H), 1.41 (t, *J* = 7.1 Hz, 6H)

^{13}C-NMR (101 MHz, DMSO-d_6): δ = 150.3, 139.7, 138.5, 129.9, 128.7, 127.3, 125.5, 122.4, 122.1, 120.8, 120.2, 118.6, 114.9, 108.9, 108.2, 56.1, 37.0, 13.7

MS (ASAP): m/z = 525.2 [M+H$^+$]

HRMS (ASAP): m/z = calculated for $C_{36}H_{33}N_2O_2$ [M+H$^+$]: 525.2542; found: 525.2535

Elemental analysis: Found C, 81.75; H, 5.99; N, 5.12 Calculated C, 82.41; H, 6.15; N, 5.34

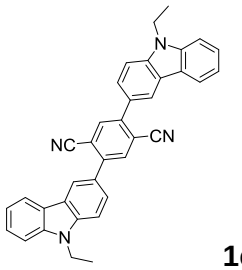

1c

Under argon, bridge **C** (95 mg, 0.25 mmol) and **3** (173 mg, 0.63 mmol) were added to a microwave vial containing $Pd(PPh_3)_4$ (21 mg, 0.02 mmol) and K_2CO_3 (242 mg, 1.75 mmol) and suspended in a degassed mixture of DMF (3 mL) and H_2O (1 mL) before the vial was sealed. The vial was then heated at 120 °C in a microwave reactor for 25 minutes. Upon cooling, the tube was opened and the reaction mixture poured into water and filtered. The solids thus obtained were then dissolved in dichloromethane and dried over $MgSO_4$. Purification was achieved by column chromatography (10% THF/hexane) followed by recrystallisation from toluene/methanol to give **1c** as a bright yellow crystalline powder (45 mg, 35%). mp. 294-297 °C (blackens)

1H-NMR (400 MHz, DMSO-d_6): δ = 8.52 (d, J = 1.8 Hz, 2H), 8.30 (s, 2H), 8.23 (d, J = 7.7 Hz, 2H), 7.88 – 7.74 (m, 4H), 7.64 (d, J = 8.2 Hz, 2H), 7.52 (ddd, J = 8.2, 7.1, 1.2 Hz, 2H), 7.34 – 7.20 (m, 2H), 4.54 (q, J = 7.1 Hz, 4H), 1.44 (t, J = 7.1 Hz, 6H)

13C-NMR (101 MHz, DMSO-d_6): δ = 143.5, 140.0, 139.8, 135.3, 126.2, 126.1, 122.7, 122.1, 121.0, 120.5, 119.2, 117.6, 114.5, 109.3, 109.2, 37.2, 13.7

MS (ASAP): m/z = 516.2 [M+2H$^+$]

HRMS (ASAP): m/z = calculated for $C_{36}H_{26}N_4$: 514.2157, found: 514.2162

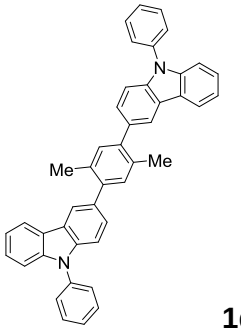

1d

Under argon, bridge **A** (66 mg, 0.25 mmol) and 9-phenyl-3-bromocarbazole **4** (202 mg, 0.63 mmol) were added to a microwave vial containing $Pd(PPh_3)_4$ (21 mg, 0.02 mmol) and K_2CO_3 (242 mg, 1.75 mmol) and suspended in a degassed mixture of DMF (3 mL) and H_2O (1 mL) before the vial was sealed. The vial was then heated at 120 °C in a microwave reactor for 25 minutes. Upon cooling, the tube was opened and the reaction mixture poured into water and filtered. The solids thus obtained were then dissolved in dichloromethane and dried over $MgSO_4$ prior to removal of solvent under reduced pressure. Purification was achieved by column chromatography (10% EtOAc/hexane) followed by recrystallisation from EtOAc/hexane to give **1d** as a white crystalline powder (41 mg, 31%). mp. 249-251 °C

N.B. Addition of a few drops of CS_2 to the NMR sample was required to inhibit aggregation and obtain well-resolved NMR spectra.

^{1}H NMR (400 MHz, DMSO-d_6): δ = 8.26 (d, J = 7.7 Hz, 2H), 8.21 (s, 2H), 7.76 – 7.67 (m, 4H), 7.70 – 7.62 (m, 4H), 7.60 – 7.51 (m, 2H), 7.51 – 7.39 (m, 8H), 7.34 – 7.26 (m, 2H), 7.28 (s, 2H), 2.39 (s, 6H)

^{13}C-NMR (101 MHz, DMSO-d_6): δ = 140.39, 140.38, 139.0, 136.9, 133.1, 132.1, 132.0, 130.0 (2C), 127.4, 127.2, 126.4 (2C), 126.1, 122.82, 122.78, 120.7, 120.5, 119.9, 109.5, 109.0, 19.9

MS (ASAP): m/z = 589.2 [M+H$^+$]

HRMS (ASAP): m/z = calculated for $C_{44}H_{33}N_2$ [M+H$^+$]: 589.2644; found: 589.2651

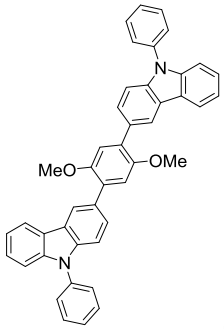

1e

Under argon, bridge **B** (98 mg, 0.25 mmol) and **4** (202 mg, 0.63 mmol) were added to a microwave vial containing $Pd(PPh_3)_4$ (21 mg, 0.02 mmol) and K_2CO_3 (242 mg, 1.75 mmol) and suspended in a degassed mixture of DMF (3 mL) and H_2O (1 mL) before the vial was sealed. The vial was then heated at 120 °C in a microwave reactor for 25 minutes. Upon cooling, the tube was opened and the reaction mixture poured into water and filtered. The solids thus obtained were then dissolved in dichloromethane and dried over $MgSO_4$ prior to removal of solvent under reduced pressure.

Purification was achieved by column chromatography (10% EtOAc/hexane) followed by recrystallisation from EtOAc/hexane to give **1e** as a white crystalline powder (74 mg, 48%). mp. 294-295 °C

N.B. Addition of a few drops of CS_2 to the NMR sample was required to inhibit aggregation and obtain well-resolved NMR spectra.

^{1}H NMR (400 MHz, DMSO-d_6): δ = 8.40 (dd, *J* = 1.7, 0.6 Hz, 2H), 8.26 (dt, *J* = 7.7, 1.0 Hz, 2H), 7.77 – 7.69 (m, 5H), 7.69 – 7.62 (m, 5H), 7.60 – 7.51 (m, 2H), 7.49 – 7.40 (m, 6H), 7.30 (ddd, *J* = 7.9, 6.0, 2.1 Hz, 2H), 7.16 (s, 2H), 3.21 (s, 6H)

^{13}C NMR (101 MHz, DMSO-d_6): δ = 150.3, 140.4, 139.1, 136.9, 130.00, 129.97 (2C), 129.8, 127.8, 127.4, 126.4 (2C), 126.0, 122.9, 122.6, 121.0, 120.4, 119.9, 114.9, 109.5, 108.8, 56.1

MS (ASAP): m/z = 621.2 [M+H$^+$]

HRMS (ASAP): m/z = calculated for $C_{44}H_{33}N_2O_2$ [M+H$^+$]: 621.2542; found: 621.2558

Elemental analysis: Found C, 84.97; H, 5.23; N, 4.38 Calculated C, 85.14; H, 5.20; N 4.51

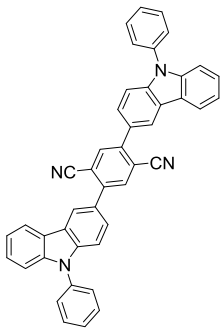

1f

Under argon, bridge **C** (95 mg, 0.25 mmol) and **4** (202 mg, 0.63 mmol) were added to a microwave vial containing $Pd(PPh_3)_4$ (21 mg, 0.02 mmol) and K_2CO_3 (242 mg, 1.75 mmol) and suspended in a degassed mixture of DMF (3 mL) and H_2O (1 mL) before the vial was sealed. The vial was then heated at 120 °C in a microwave reactor for 25 minutes. Upon cooling, the tube was opened and the reaction mixture poured into water and filtered. The solids thus obtained were then dissolved in dichloromethane and dried over $MgSO_4$ prior to removal of solvent under reduced pressure. Purification was achieved by column chromatography (0-20% toluene/hexane) followed by recrystallisation from toluene/methanol to give **1f** as a yellow crystalline powder (50 mg, 33%). mp. 347-348 °C (luminescence observed between 313-319 °C)

N.B. Addition of a few drops of CS_2 to the NMR sample was required to inhibit aggregation and obtain well-resolved NMR spectra.

It was not possible to obtain a solution of suitable concentration for ^{13}C-NMR spectroscopy.

^{1}H NMR (400 MHz, DMSO-d_6): δ = 8.64 (d, *J* = 1.8 Hz, 2H), 8.36 (s, 2H), 8.33 (d, *J* = 7.8 Hz, 2H), 7.81 (dd, *J* = 8.6, 1.9 Hz, 2H), 7.77 – 7.71 (m, 4H), 7.71 – 7.66 (m, 4H), 7.62 – 7.57 (m, 2H), 7.56 (d, *J* = 8.5 Hz, 2H), 7.54 – 7.48 (m, 2H), 7.45 (d, *J* = 8.2 Hz, 2H), 7.39 – 7.34 (m, 2H)

MS (ASAP): m/z = 611.2 [M+H$^+$]

HRMS (ASAP): m/z = calculated for $C_{44}H_{27}N_4$ $[M+H]^+$: 611.2236; found: 611.2247

Elemental analysis: Found C, 85.99; H, 4.27; N, 9.01 Calculated C, 86.53; H, 4.29; N 9.17

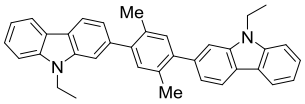

2a

Under argon, bridge **A** (108 mg, 0.41 mmol) and 9-ethyl-2-bromocarbazole **5** (250 mg, 0.91 mmol) were added to a microwave vial containing $Pd(PPh_3)_4$ (35 mg, 0.03 mmol) and K_2CO_3 (400 mg, 2.87 mmol) and suspended in a degassed mixture of DMF (3 mL) and H_2O (1 mL) before the vial was sealed. The vial was then heated at 120 °C in a microwave reactor for 25 minutes. Upon cooling, the tube was opened and the reaction mixture poured into water and filtered. The solids thus obtained were then dissolved in dichloromethane and dried over $MgSO_4$ prior to removal of solvent under reduced pressure. Purification was achieved by column chromatography (10% THF/hexane) followed by recrystallisation from toluene/methanol to give **2a** as a white crystalline solid (61 mg, 30%). mp. >256 °C (blackens)

N.B. Addition of a few drops of CS_2 to the NMR sample was required to inhibit aggregation and obtain well-resolved NMR spectra.

^{1}H NMR (400 MHz, DMSO-d_6): δ = 8.16 (d, *J* = 8.0 Hz, 2H), 8.14 (d, *J* = 7.4 Hz, 2H), 7.58 (d, *J* = 8.2 Hz, 2H), 7.54 (d, *J* = 1.4 Hz, 2H), 7.46 (ddd, *J* = 8.2, 7.1, 1.2 Hz, 2H), 7.30 (s, 2H), 7.24 – 7.18 (m, 2H), 7.21 (dd, *J* = 7.9, 1.4 Hz, 2H), 4.50 (q, *J* = 7.1 Hz, 4H), 2.38 (s, 6H), 1.41 (t, *J* = 7.1 Hz, 6H)

^{13}C NMR (101 MHz, DMSO-d_6): δ = 140.9, 139.8, 139.4, 138.7, 132.0, 131.8, 125.4, 122.1, 121.0, 120.1, 120.0, 119.7, 118.6, 109.2, 108.8, 36.9, 19.9, 13.7

MS (ASAP): m/z = 493.3 $[M+H^+]$

HRMS (ASAP$^+$): m/z = calculated for $C_{36}H_{33}N_2$ $[M+H^+]$: 493.2644; found: 493.2639

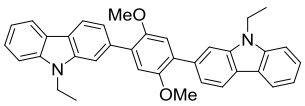

2b

Under argon, bridge **B** (160 mg, 0.41 mmol) and **5** (250 mg, 0.91 mmol) were added to a microwave vial containing $Pd(PPh_3)_4$ (35 mg, 0.03 mmol) and K_2CO_3 (400 mg, 2.87 mmol) and suspended in a degassed mixture of DMF (3 mL) and H_2O (1 mL) before the vial was sealed. The vial was then heated at 120 °C in a microwave reactor for 25 min.

Upon cooling, the tube was opened and the reaction mixture poured into water and extracted with CH_2Cl_2 (3 x 25 mL). The combined organic extracts were washed with 2M HCl (2 x 25 mL) and water (2 x 25 mL) and dried over $MgSO_4$. The drying agent was removed by filtration and charcoal was added to the filtrate which was then stirred for 30 minutes before being filtered over celite. Solvent was removed under reduced pressure. Purification was by recrystallisation from toluene/methanol to give **2b** as a white crystalline solid (61 mg, 31%). mp. 287-289 °C

^{1}H NMR (400 MHz, $CDCl_3$): δ = 8.17 (d, *J* = 8.0 Hz, 2H), 8.14 (d, *J* = 7.8 Hz, 2H), 7.72 – 7.67 (m, 2H), 7.52 – 7.41 (m, 8H), 7.26 – 7.22 (m, 2H), 7.18 (s, 2H), 4.44 (q, *J* = 7.2 Hz, 6H), 3.86 (s, 6H), 1.47 (t, *J* = 7.2 Hz, 6H)

^{13}C NMR (101 MHz, $CDCl_3$): δ = 151.1, 140.6, 140.1, 136.0, 131.5, 125.7, 123.1, 122.2, 120.7, 120.6, 120.1, 119.0, 115.8, 109.7, 108.6, 56.9, 37.7, 14.0

MS (ASAP): m/z = 525.2 [M+H$^+$]

HRMS (ASAP): m/z = calculated for $C_{36}H_{33}N_2O_2$ [M+H$^+$]: 525.2542; found:525.2559

Elemental analysis: Found C, 82.13; H, 6.13; N, 5.22 Calculated C, 82.41; H, 6.15; N, 5.34

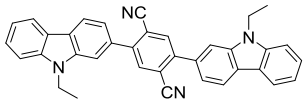

2c

Under argon, bridge **C** (156 mg, 0.41 mmol) and **5** (250 mg, 0.91 mmol) were added to a microwave vial containing $Pd(PPh_3)_4$ (35 mg, 0.03 mmol) and K_2CO_3 (400 mg, 2.87 mmol) and suspended in a degassed mixture of DMF (3 mL) and H_2O (1 mL) before the vial was sealed. The vial was then heated at 120 °C in a microwave reactor for 25 minutes. Upon cooling, the tube was opened and the reaction mixture poured into water and filtered. The solids thus obtained were then dissolved in dichloromethane and dried over $MgSO_4$ prior to removal of solvent under reduced pressure. Purification was achieved by column chromatography (0-20% toluene/hexane) followed by recrystallisation from toluene/methanol to give **2c** as yellow crystals (38 mg, 18%). mp. >310 °C (blackens)

N.B. Addition of a few drops of CS_2 to the NMR sample was required to inhibit aggregation and obtain well-resolved NMR spectra.

^{1}H NMR (400 MHz, DMSO-d_6): δ = 8.42 (s, 2H), 8.33 (d, *J* = 7.8 Hz, 2H), 8.22 (d, *J* = 7.7 Hz, 2H), 7.99 (d, *J* = 1.7 Hz, 2H), 7.65 (d, *J* = 8.2 Hz, 2H), 7.61 – 7.45 (m, 4H), 7.26 (td, *J* = 7.5, 0.9 Hz, 2H), 4.56 (q, *J* = 7.0 Hz, 4H), 1.44 (t, *J* = 7.1 Hz, 6H)

^{13}C NMR (101 MHz, DMSO-d_6): δ = 143.9, 140.3, 139.4, 135.4, 132.7, 126.3, 123.0, 121.6, 120.7, 120.6, 119.3, 119.1, 117.5, 114.8, 109.7, 109.1, 37.1, 13.7

MS (ASAP): m/z = 515.2 [M+H$^+$]

HRMS (ASAP): m/z = calculated for $C_{36}H_{27}N_4$ [M+H$^+$]: 515.2236; found: 515.2222

Elemental analysis: Found C, 83.63; H, 5.09; N 10.71, Calculated C, 84.02; H, 5.09; N, 10.89

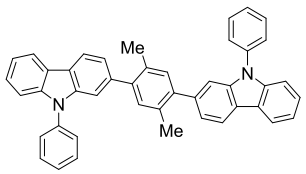

2d

Under argon, bridge **A** (108 mg, 0.41 mmol) and 9-phenyl-2-bromocarbazole **6** (293 mg, 0.91 mmol) were added to a microwave vial containing $Pd(PPh_3)_4$ (35 mg, 0.03 mmol) and K_2CO_3 (400 mg, 2.87 mmol) and suspended in a degassed mixture of DMF (3 mL) and H_2O (1 mL) before the vial was sealed. The vial was then heated at 120 °C in a microwave reactor for 25 minutes. Upon cooling, the tube was opened and the reaction mixture poured into water and filtered. The solids thus obtained were then dissolved in dichloromethane and dried over $MgSO_4$ prior to removal of solvent under reduced pressure. Purification was achieved by column chromatography (10% EtOAc/hexane) followed by recrystallisation from toluene/methanol to give **2d** as a white crystalline solid (100 mg, 41%). mp. 178-181 °C

N.B. Addition of a few drops of CS_2 to the NMR sample was required to inhibit aggregation and obtain well-resolved NMR spectra.

^{1}H NMR (400 MHz, DMSO-d_6): δ = 8.25 – 8.19 (m, 4H), 7.70 – 7.65 (m, 4H), 7.65 – 7.59 (m, 4H), 7.56 – 7.48 (m, 2H), 7.48 – 7.37 (m, 4H), 7.34 – 7.26 (m, 4H), 7.27 (dd, *J* = 7.9, 1.5 Hz, 2H), 7.16 (s, 2H), 2.29 (s, 6H)

^{13}C NMR (101 MHz, DMSO-d_6): δ = 141.3, 141.0, 140.7, 139.8, 137.4, 132.6, 132.3, 130.6 (2C), 128.0, 127.1 (2C), 126.5, 123.3, 122.2, 121.9, 120.9, 120.64, 120.55, 110.4, 110.0, 20.4

MS (ASAP): m/z = 589.2 [M+H$^+$]

HRMS (ASAP): m/z = calculated for $C_{44}H_{32}N_2$ [M$^+$]: 588.2565; found: 588.2594

Elemental analysis: Found C, 89.72; H, 5.47; N 4.67, Calculated C, 89.76; H, 5.48; N, 4.76.

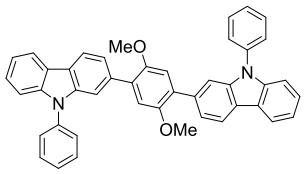

2e

Under argon, bridge **B** (160 mg, 0.41 mmol) and **6** (293 mg, 0.91 mmol) were added to a microwave vial containing $Pd(PPh_3)_4$ (35 mg, 0.03 mmol) and K_2CO_3 (400 mg, 2.87 mmol) and suspended in a degassed mixture of DMF (3 mL) and H_2O (1 mL) before the vial was sealed. The vial was then heated at 120 °C in a microwave reactor for 25 minutes. Upon cooling, the tube was opened and the reaction mixture poured into water and extracted with $CHCl_3$ (3 x 25 mL). The combined organic extracts were washed with 2M HCl (2 x 25 mL) and water (2 x 25 mL) and dried over $MgSO_4$. The drying agent was removed by filtration and charcoal was added to the filtrate which was then stirred for 30 minutes before being filtered over celite. Solvent was removed under reduced pressure. Purification was by recrystallisation from toluene/methanol to give **2e** as a white crystalline solid (118 mg, 46%). mp. 216-219 °C

N.B. Addition of a few drops of CS_2 to the NMR sample was required to inhibit aggregation and obtain well-resolved NMR spectra.

^{1}H NMR (400 MHz, DMSO-d_6): δ = 8.21 (dd, *J* = 8.1, 0.7 Hz, 2H), 8.21 (dt, *J* = 7.7, 1.1 Hz, 2H), 7.73 – 7.62 (m, 8H), 7.59 (dd, *J* = 1.5, 0.6 Hz, 2H), 7.55 – 7.49 (m, 2H), 7.46 (dd, *J* = 8.1, 1.5 Hz, 2H), 7.44 – 7.41 (m, 4H), 7.29 (ddd, *J* = 8.0, 4.6, 3.4 Hz, 2H), 7.05 (s, 2H), 3.75 (s, 6H)

^{13}C NMR (101 MHz, DMSO-d_6): δ = 150.8, 141.1, 140.5, 137.5, 136.4, 130.8, 130.5 (2C), 127.9, 127.0 (2C), 126.5, 123.3, 122.3, 122.2, 120.9, 120.6, 120.3, 115.5, 111.0, 110.0, 56.7

MS (ASAP): m/z = 621.2 [M+H$^+$]

HRMS (ASAP): m/z = calculated for $C_{44}H_{33}N_2O_2$ [M+H$^+$]: 621.2542; found: 621.2557

Elemental analysis: Found C, 85.04; H, 5.27; N 4.32, Calculated C, 85.14; H, 5.20; N 4.51

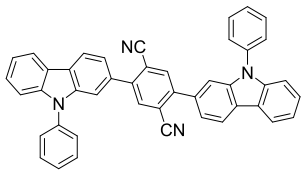

2f

Under argon, bridge **C** (156 mg, 0.41 mmol) and **6** (293 mg, 0.91 mmol) were added to a microwave vial containing $Pd(PPh_3)_4$ (35 mg, 0.03 mmol) and K_2CO_3 (400 mg, 2.87 mmol) and suspended in a degassed mixture of DMF (3 mL) and H_2O (1 mL) before the vial was sealed. The vial was then heated at 120 °C in a microwave reactor for 25 minutes. Upon cooling, the tube was opened and the reaction mixture poured into water and filtered. The solids thus obtained were then dissolved in dichloromethane and dried over $MgSO_4$ prior to removal of solvent under reduced pressure. Purification was achieved by column chromatography (0-20% toluene/hexane) followed by recrystallisation from toluene/methanol to give **2f** as yellow crystals (99 mg, 40%). Mp. 320-322 °C (luminescence observed above 290 °C)

N.B. Addition of a few drops of CS_2 to the NMR sample was required to inhibit aggregation and obtain well-resolved NMR spectra.

^{1}H-NMR (400 MHz, DMSO-d_6): δ = 8.43 (dd, J = 8.1, 0.6 Hz, 1H), 8.36 – 8.28 (m, 2H), 7.73 – 7.68 (m, 5H), 7.59 (dd, J = 8.1, 1.6 Hz, 1H), 7.58 – 7.52 (m, 1H), 7.50 (dd, J = 6.8, 1.3 Hz, 1H), 7.48 – 7.44 (m, 1H), 7.35 (ddd, J = 8.0, 6.7, 1.3 Hz, 1H)

^{13}C NMR (101 MHz, DMSO-d_6): δ = 192.4, 143.8, 140.8, 139.8, 136.4, 135.2, 133.3, 130.1 (2C), 127.6, 126.9, 126.5 (2C), 123.5, 122.2, 121.0, 120.7, 120.4, 117.2, 114.8, 110.2, 109.7

MS (ASAP): m/z = 611.2 [M+H$^+$].

HRMS (ASAP): m/z = calculated for $C_{44}H_{27}N_4$ [M+H]$^+$: 611.2236; found: 611.2257.

Elemental analysis: Found C, 86.51; H, 4.33; N, 8.99 Calculated C, 86.53; H, 4.29; N 9.17

Copies of ^{1}H NMR Spectra:

1a

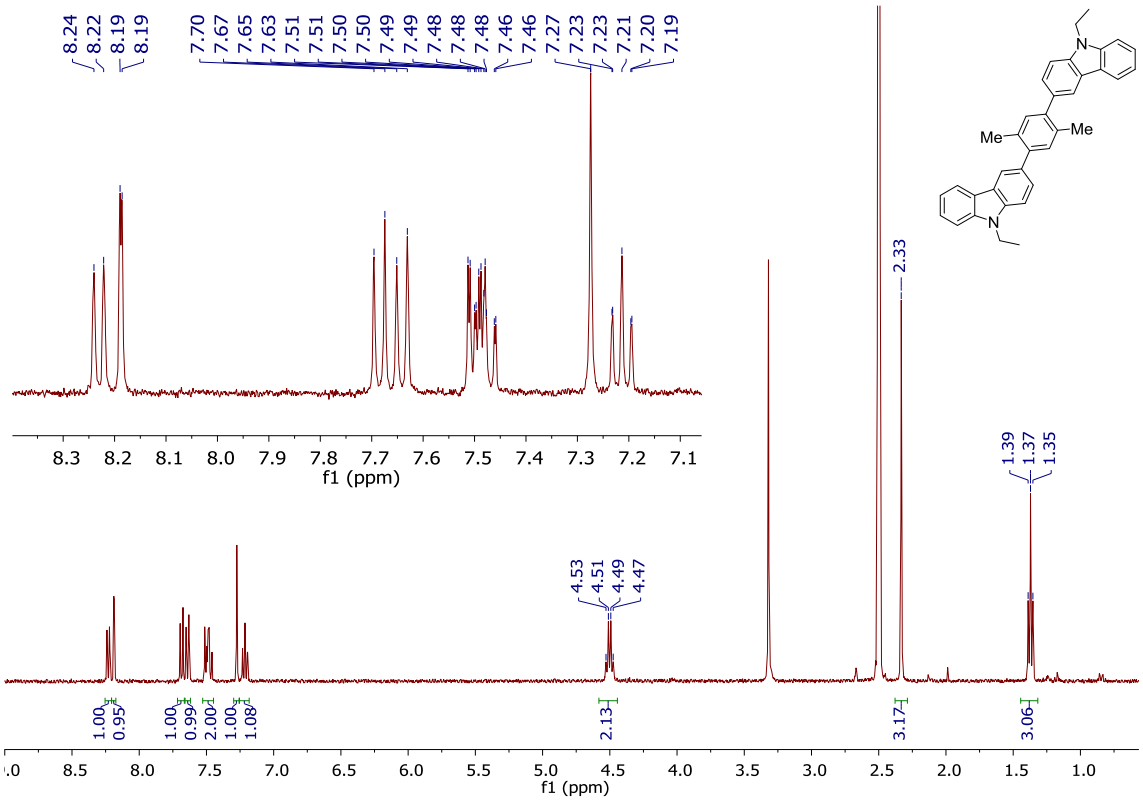

1b

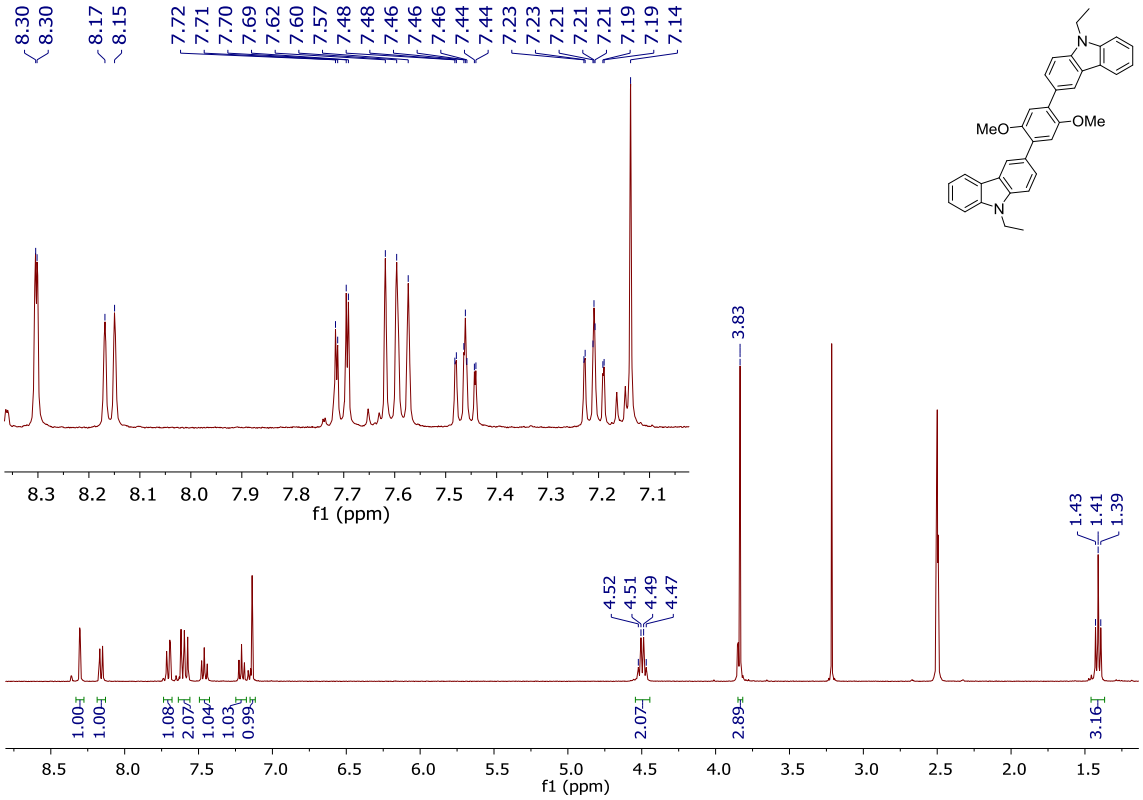
8.30
8.30
8.17
8.15
7.72
7.71
7.70
7.69
7.62
7.60
7.57
7.48
7.48
7.46
7.46
7.46
7.44
7.44
7.23
7.23
7.21
7.21
7.21
7.19
7.19
7.14
MeO
OMe
N
3.83
1.43
1.41
1.39
4.52
4.51
4.49
4.47
1.00
1.00
1.08
2.07
1.04
1.03
0.99
2.07
2.89
3.16
f1 (ppm)

1c

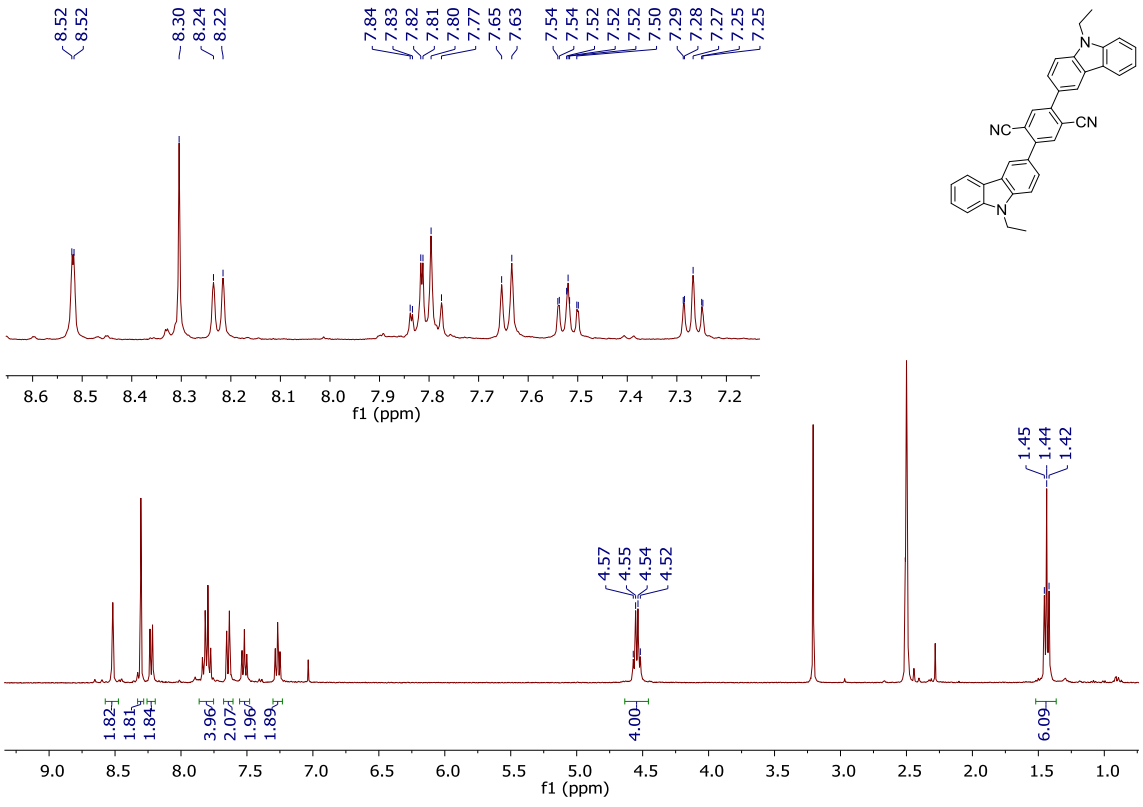
8.52
8.52
8.30
8.24
8.22
7.84
7.83
7.82
7.81
7.80
7.77
7.65
7.63
7.54
7.54
7.52
7.52
7.52
7.50
7.29
7.28
7.27
7.25
7.25
NC
CN
N
1.45
1.44
1.42
4.57
4.55
4.54
4.52
1.82
1.81
1.84
3.96
2.07
1.96
1.89
4.00
6.09
f1 (ppm)

1d

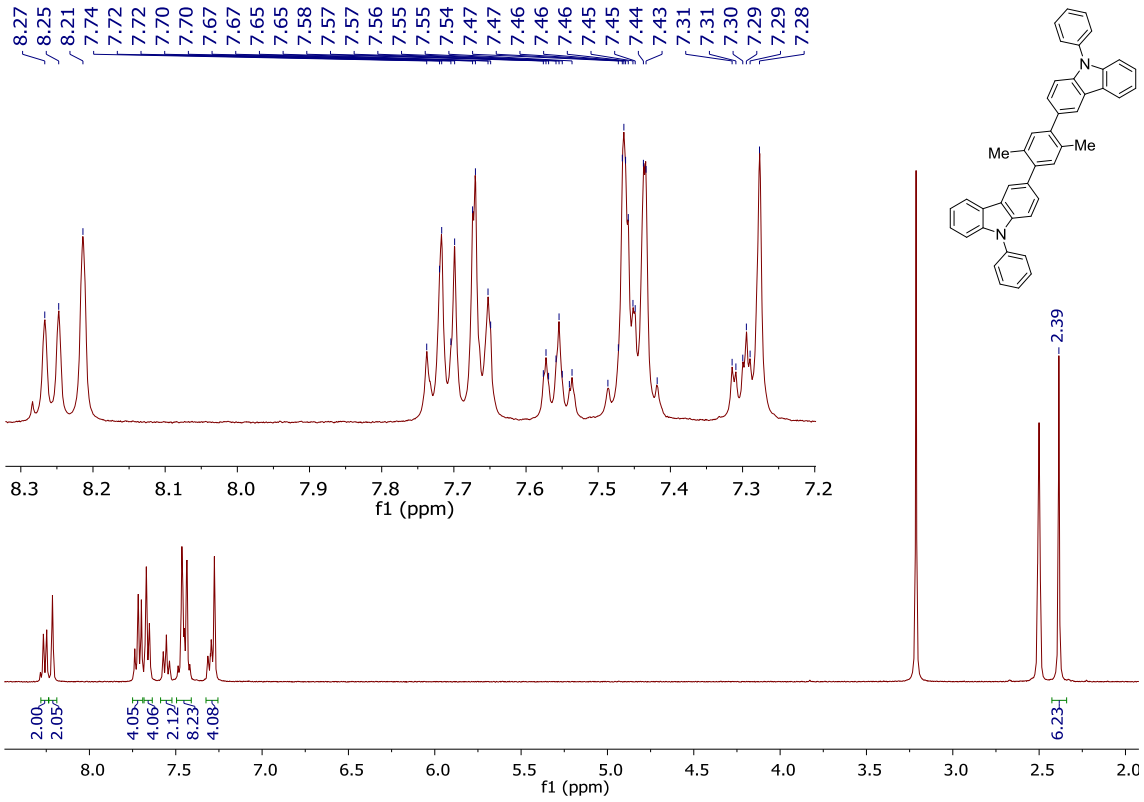
8.27 8.25 8.21 7.74 7.72 7.72 7.70 7.70 7.67 7.65 7.65 7.58 7.57 7.57 7.56 7.55 7.55 7.54 7.47 7.47 7.46 7.46 7.45 7.45 7.44 7.43 7.31 7.31 7.30 7.29 7.29 7.28
Me
Me
N
N
2.39
f1 (ppm)
2.00 2.05 4.05 4.06 2.12 8.23 4.08 6.23
f1 (ppm)

1e

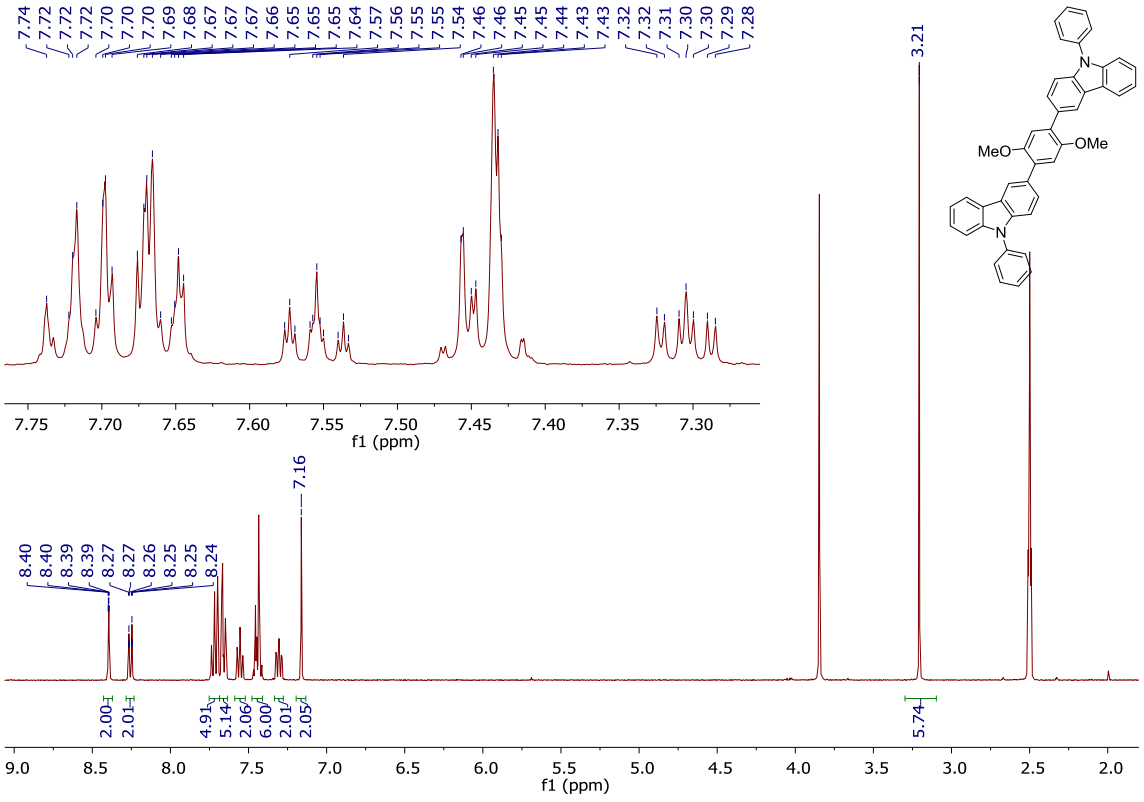
7.74 7.72 7.72 7.72 7.70 7.70 7.70 7.69 7.68 7.67 7.67 7.67 7.66 7.65 7.65 7.65 7.64 7.57 7.56 7.55 7.55 7.54 7.46 7.46 7.45 7.45 7.44 7.43 7.43 7.32 7.32 7.31 7.30 7.30 7.29 7.28
3.21
MeO
OMe
N
N
f1 (ppm)
7.16
8.40 8.40 8.39 8.39 8.27 8.27 8.26 8.25 8.25 8.24
2.00 2.01 4.91 5.14 2.06 6.00 2.01 2.05 5.74
f1 (ppm)

1f

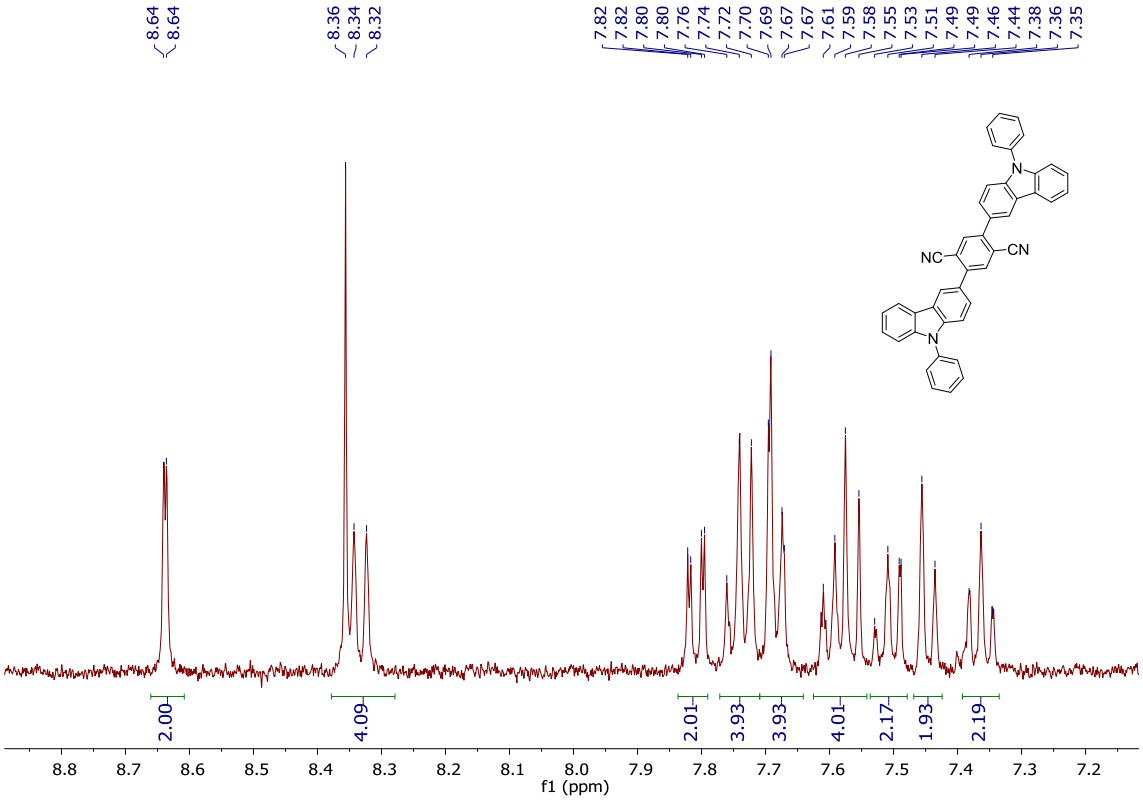
8.64
8.64
8.36
8.34
8.32
7.82
7.82
7.80
7.80
7.76
7.74
7.72
7.70
7.69
7.67
7.67
7.61
7.59
7.58
7.55
7.53
7.51
7.49
7.49
7.46
7.44
7.38
7.36
7.35
N
NC
CN
N
2.00
4.09
2.01
3.93
3.93
4.01
2.17
1.93
2.19
8.8
8.7
8.6
8.5
8.4
8.3
8.2
8.1
8.0
7.9
7.8
7.7
7.6
7.5
7.4
7.3
7.2
f1 (ppm)

2a

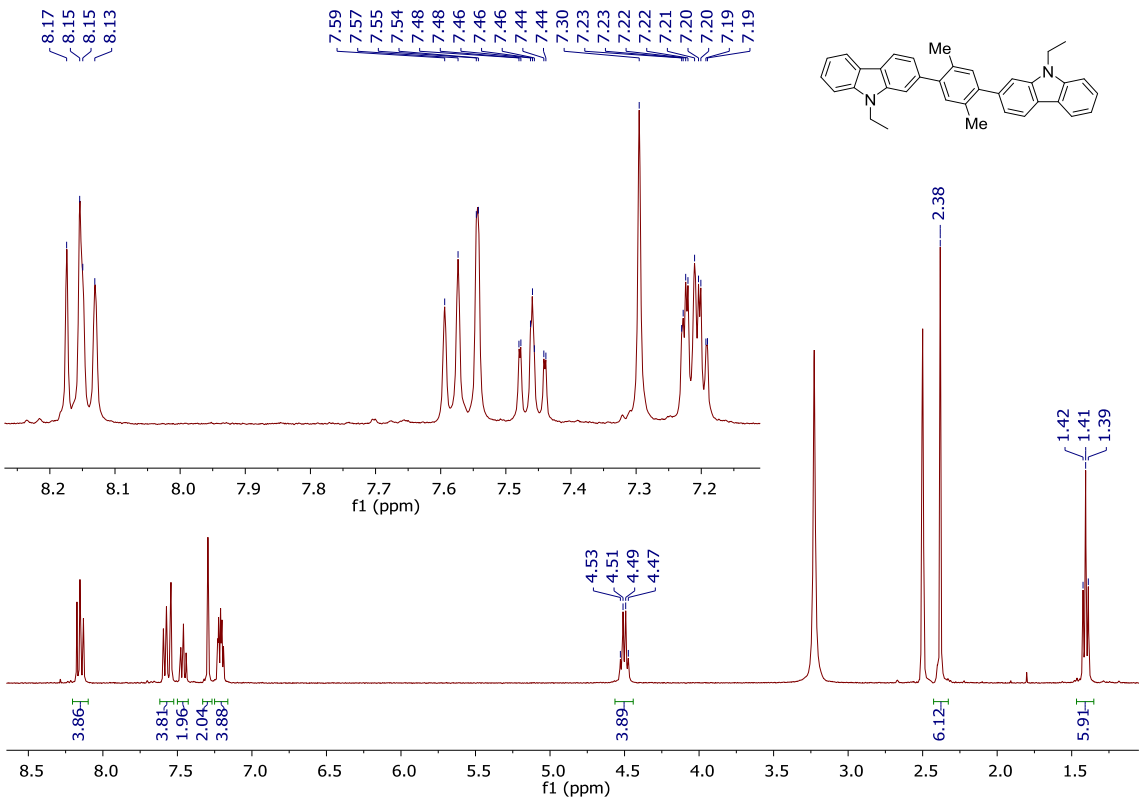
8.17
8.15
8.15
8.13
7.59
7.57
7.55
7.54
7.48
7.48
7.46
7.46
7.46
7.44
7.44
7.30
7.23
7.23
7.22
7.22
7.21
7.20
7.20
7.19
7.19
Me
N
N
Me
2.38
1.42
1.41
1.39
4.53
4.51
4.49
4.47
3.86
3.81
1.96
2.04
3.88
3.89
6.12
5.91
8.2
8.1
8.0
7.9
7.8
7.7
7.6
7.5
7.4
7.3
7.2
f1 (ppm)
8.5
8.0
7.5
7.0
6.5
6.0
5.5
5.0
4.5
4.0
3.5
3.0
2.5
2.0
1.5
f1 (ppm)

2b

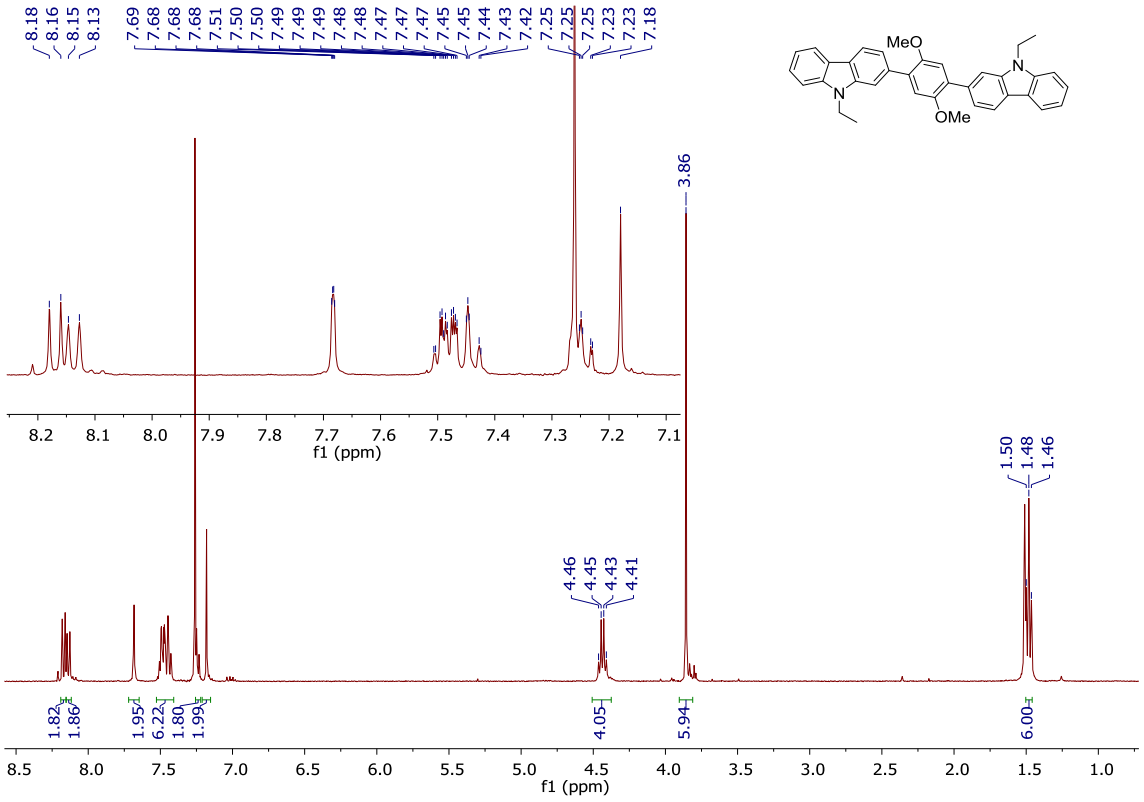
8.18
8.16
8.15
8.13
7.69
7.68
7.68
7.68
7.51
7.50
7.50
7.49
7.49
7.49
7.48
7.48
7.47
7.47
7.47
7.45
7.45
7.44
7.43
7.42
7.25
7.25
7.25
7.23
7.23
7.18
MeO
OMe
N
N
3.86
f1 (ppm)
1.50
1.48
1.46
4.46
4.45
4.43
4.41
1.82
1.86
1.95
6.22
1.80
1.99
4.05
5.94
6.00
f1 (ppm)

2c

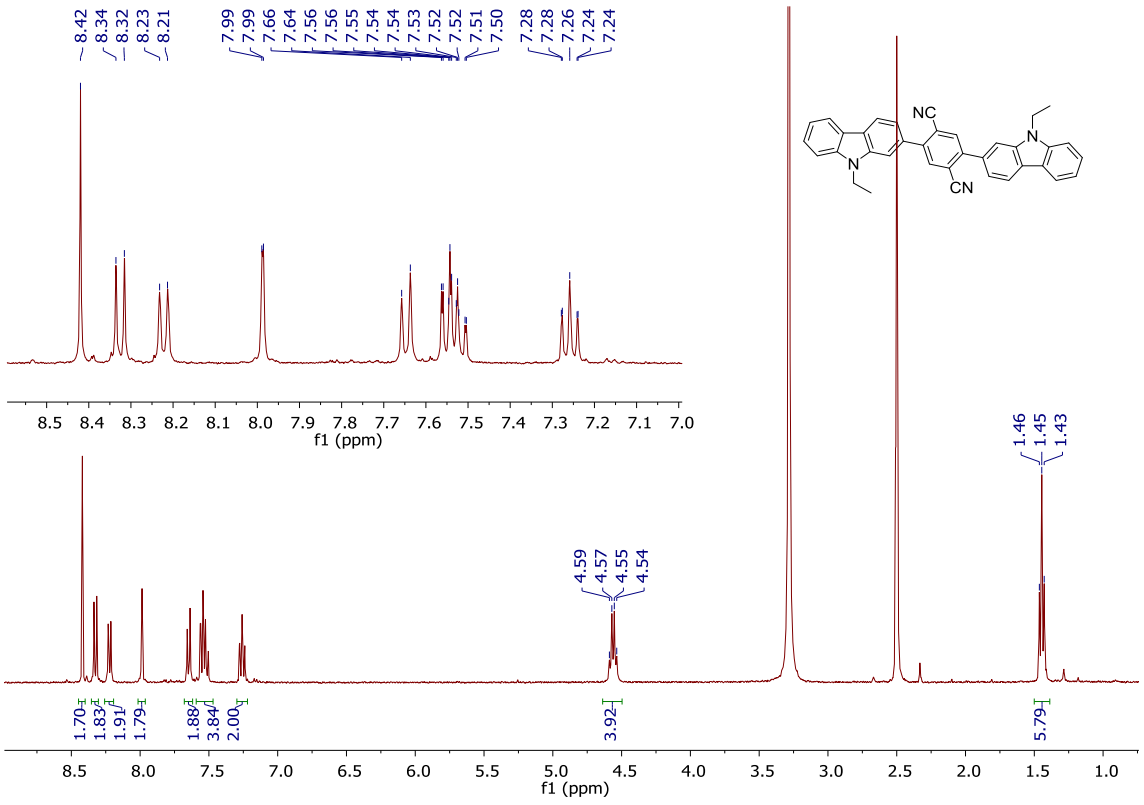
8.42
8.34
8.32
8.23
8.21
7.99
7.99
7.66
7.64
7.56
7.56
7.55
7.54
7.54
7.53
7.52
7.52
7.51
7.50
7.28
7.28
7.26
7.24
7.24
NC
CN
N
N
f1 (ppm)
1.46
1.45
1.43
4.59
4.57
4.55
4.54
1.70
1.83
1.91
1.79
1.88
3.84
2.00
3.92
5.79
f1 (ppm)

2d

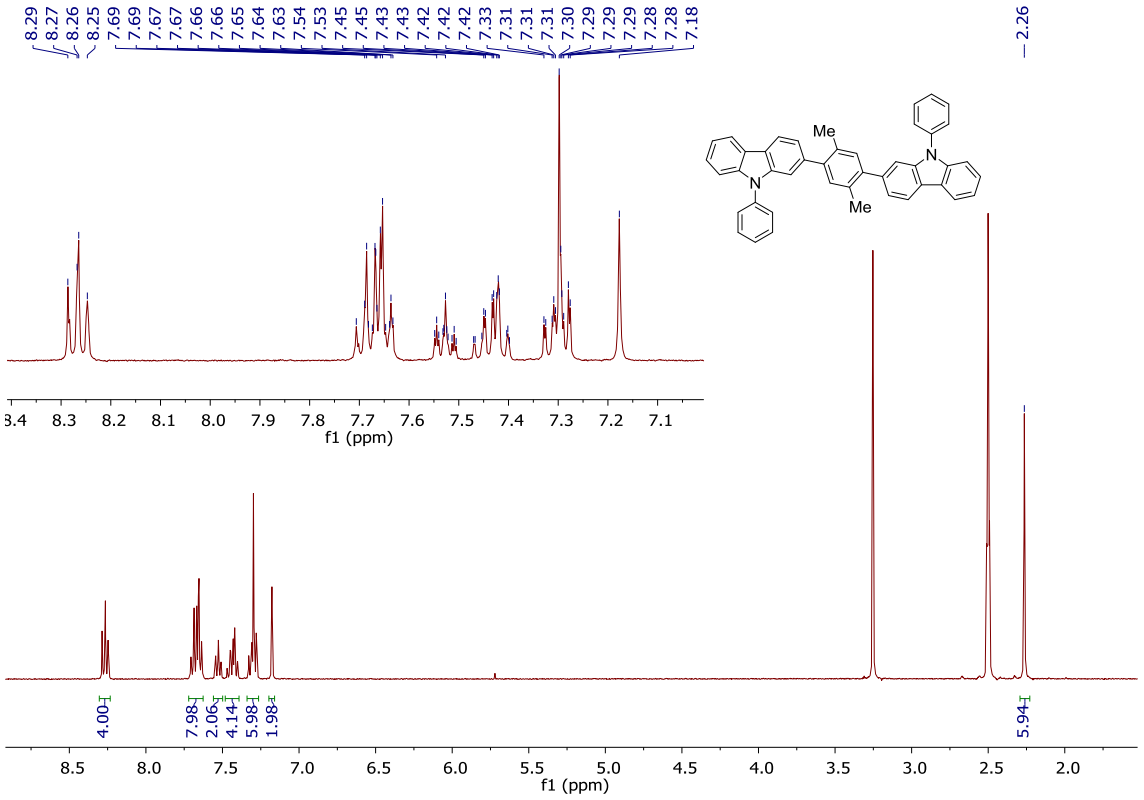
8.29 8.27 8.26 8.25 7.69 7.69 7.67 7.67 7.66 7.66 7.65 7.64 7.63 7.54 7.53 7.45 7.45 7.43 7.43 7.42 7.42 7.42 7.33 7.31 7.31 7.31 7.30 7.29 7.29 7.29 7.28 7.28 7.18
2.26
Me
Me
N
N
f1 (ppm)
4.00 7.98 2.06 4.14 5.98 1.98 5.94
f1 (ppm)

2e

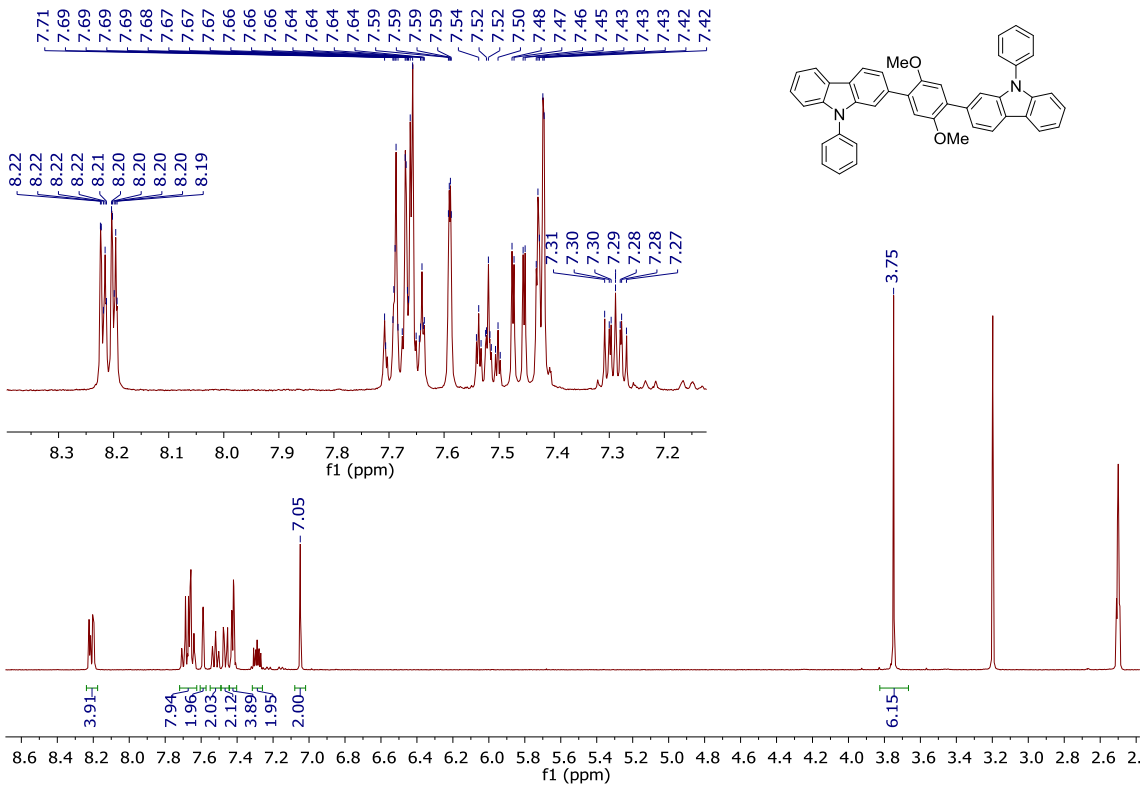
7.71 7.69 7.69 7.69 7.68 7.67 7.67 7.67 7.66 7.66 7.66 7.64 7.64 7.64 7.64 7.59 7.59 7.59 7.59 7.54 7.52 7.52 7.50 7.48 7.47 7.46 7.45 7.43 7.43 7.43 7.42 7.42
8.22 8.22 8.22 8.22 8.21 8.20 8.20 8.20 8.20 8.19
7.31 7.30 7.30 7.29 7.28 7.28 7.27
MeO
OMe
N
N
3.75
f1 (ppm)
7.05
3.91 7.94 1.96 2.03 2.12 3.89 1.95 2.00 6.15
f1 (ppm)

2f

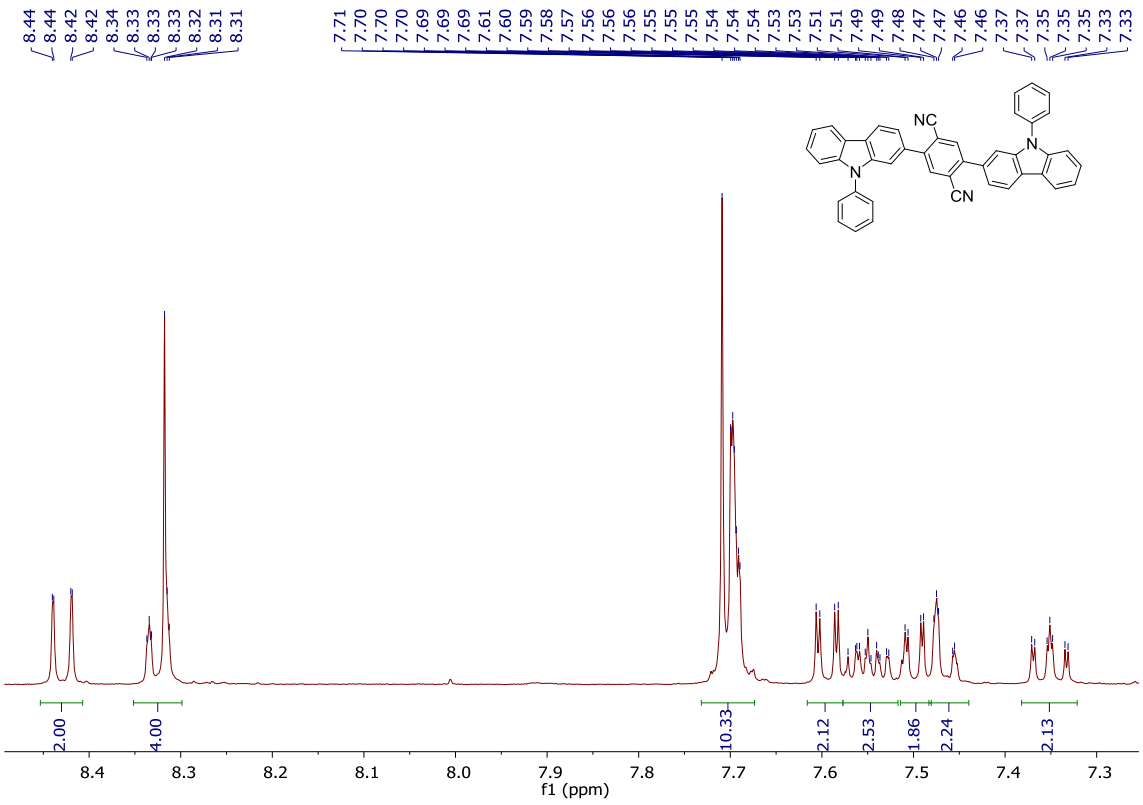

X-ray crystallography

The X-ray diffraction experiment for **1a** was carried out on a Bruker 3-circle D8 Venture diffractometer with a PHOTON 100 CMOS area detector, using Cu-K_α radiation from a IμS microsource with focussing mirrors, for **1c** on an Xcalibur κ-diffractometer with a Sapphire3 CCD area detector, using Mo-K_α radiation from an Enhance (Mo) source. Crystals were cooled to 120 K using Cryostream (Oxford Cryosystems) open-flow N_2 gas cryostats. The structures were solved by direct methods using SHELXS 2013/1 software,[1] and refined by full-matrix least squares using SHELXL 2014/7[2] and OLEX2[3] software. Crystal data have been deposited with Cambridge Structural Database as CCDC-1547241 (**1a**) and 1547242 (**1c**).

Absorption Spectra

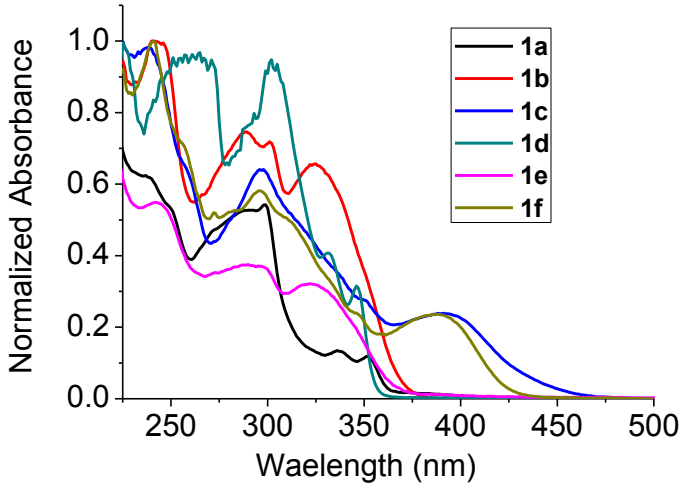

Figure S1. Absorption spectra for series 1 in zeonex (1:50 w/w) at room temperature

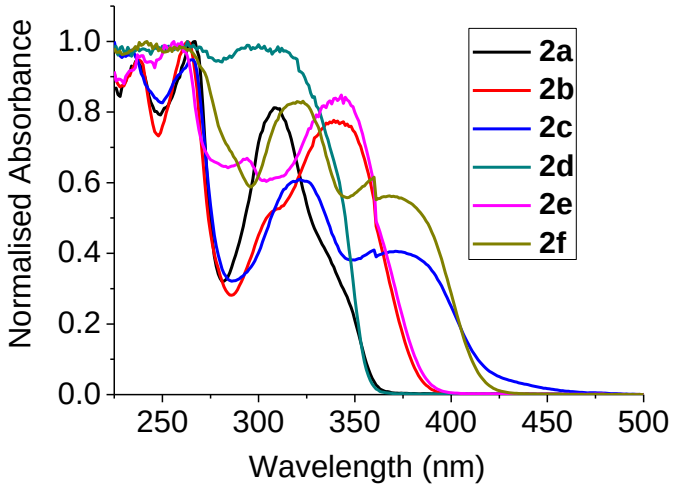

Figure S2. Absorption spectra for series 2 in zeonex (1:50 w/w) at room temperature. .

Computational studies

	LUMO+2 (eV)	LUMO+1 (eV)	LUMO (eV)	HOMO (eV)	HOMO-1 (eV)	HOMO-2 (eV)	E_g (eV)
7	-0.510	-0.574	-0.602	-4.882	-5.257	-5.539	4.280
1a	-0.266	-0.542	-0.558	-4.976	-5.205	-5.512	4.418
1b	-0.404	-0.473	-0.571	-4.798	-5.198	-5.413	4.227
1c	-0.850	-1.072	-1.978	-5.346	-5.542	-5.825	3.368
8	-0.579	-0.598	-0.668	-4.933	-5.283	-5.585	4.265
1d	-0.438	-0.568	-0.586	-5.023	-5.236	-5.56	4.437
1e	-0.453	-0.545	-0.622	-4.850	-5.229	-5.457	4.228
1f	-0.857	-1.112	-2.000	-5.366	-5.542	-5.854	3.366
9	0.088	-0.544	-1.080	-5.161	-5.255	-5.255	4.081
2a	0.168	-0.544	-0.858	-5.227	-5.229	-5.261	4.369
2b	0.211	-0.488	-0.999	-5.044	-5.128	-5.249	4.045
2c	-0.915	-1.390	-2.141	-5.508	-5.509	-5.672	3.367
10	-0.356	-0.556	-1.093	-5.179	-5.272	-5.274	4.086
2d	-0.336	-0.557	-0.875	-5.246	-5.248	-5.282	4.371
2e	-0.389	-0.504	-1.013	-5.062	-5.149	-5.271	4.049
2f	-0.908	-1.372	-2.121	-5.504	-5.505	-5.686	3.383

Table S1 Calculated (B3LYP/6-31G*) frontier orbital energy levels of compounds **1a-f**, **2a-f** and **7-10**.

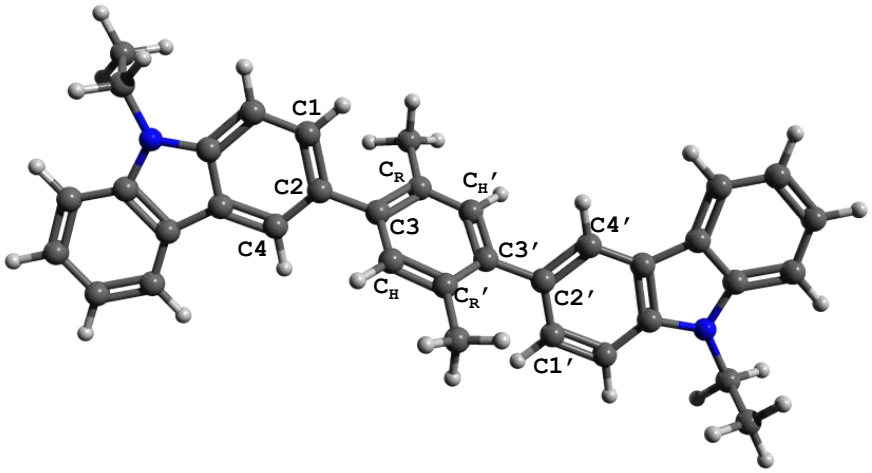

	τ_1 (°)	τ_2 (°)	τ_1' (°)	τ_2' (°)
7	37.2	37.2	—	—
1a	55.1	52.4	—	—
1b	45.9	42.3	43.5	41.8
1c	45.4	43.5	—	—
8	36.9	37.2	—	—
1d	55.1	52.2	—	—
1e	46.1	42.2	43.3	41.7
1f	45.8	43.7	—	—
9	37.4	37.2	—	—
2a	55.7	53.0	—	—
2b	46.6	42.9	43.9	42.2
2c	46.4	44.3	—	—
10	36.4	36.4	—	—
2d	54.8	52.5	—	—
2e	46.0	42.6	43.3	41.6
2f	45.7	43.9	—	—

Table S2. Calculated dihedral angles between bridge and carbazole for compounds **1**, **2** and **7**−**10** (τ_1 = ∠C1C2C3C_R, τ_2 = ∠C4C2C3C_H, τ_1' = ∠C1'C2'C3'C_R', τ_2' = ∠C4'C2'C3'C_H'). The structure of **1a** is shown to illustrate the numbering system adopted. For compounds **1b**,**e** and **2b**,**e** τ_1/τ_2 refer to the MeO_{eq} side of the bridge and τ_1'/τ_2' refer to the MeO_{ax} side of the bridge.

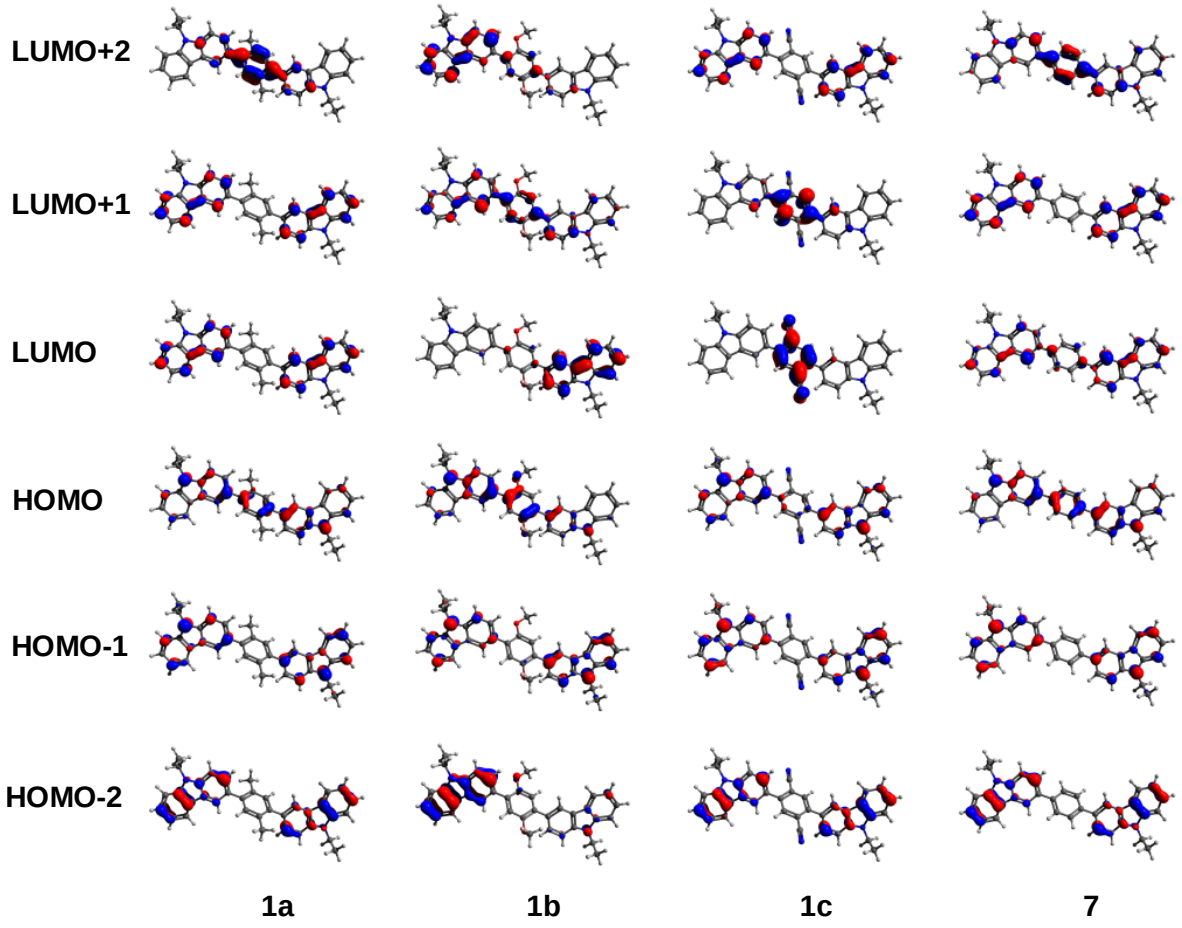

Figure S3 Frontier molecular orbital plots for the complete 3-substituted *N*-ethylcarbazolyl series **1a**−**c** and **7**.

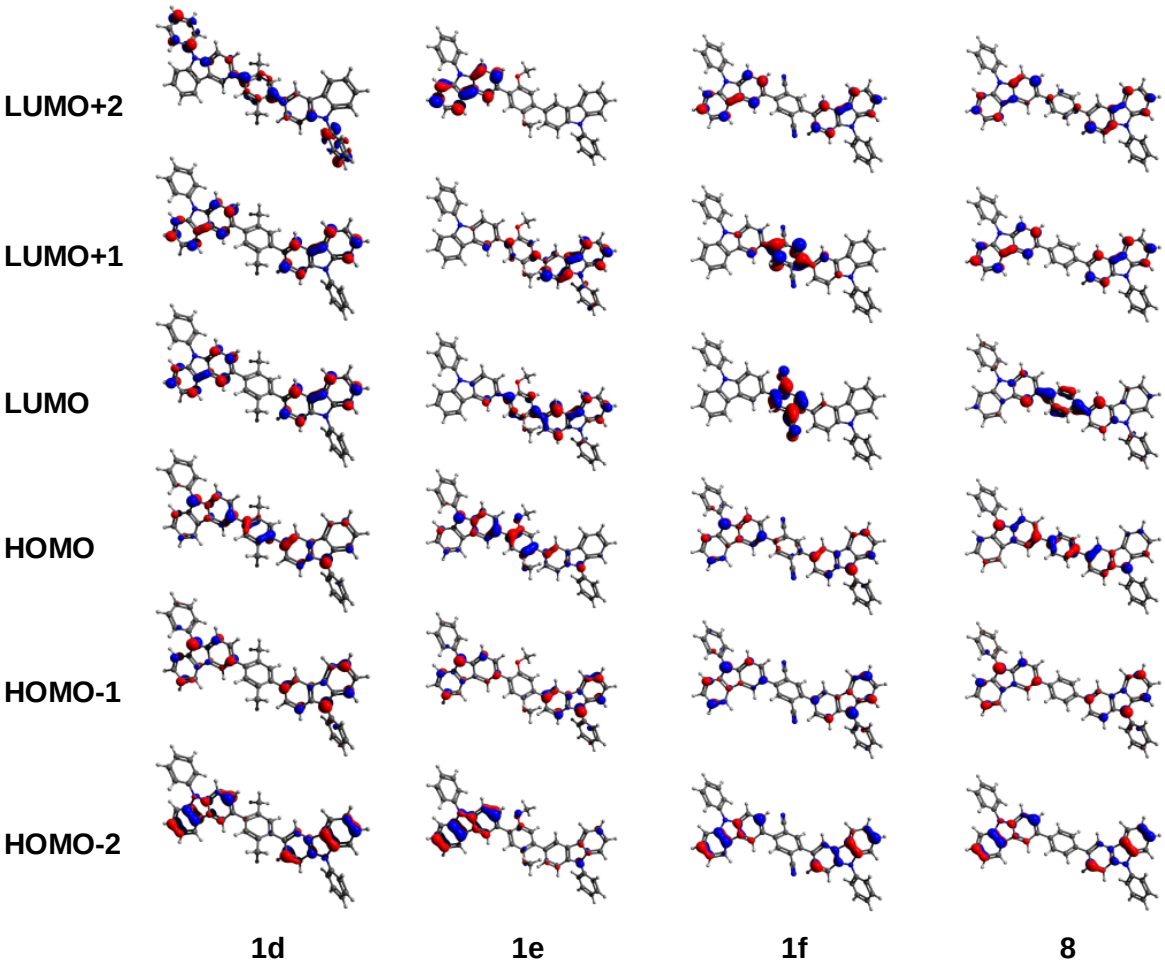

Figure S4 Frontier molecular orbital plots for the complete 3-substituted *N*-phenylcarbazolyl series **1d**–**f** and model compound **8**.

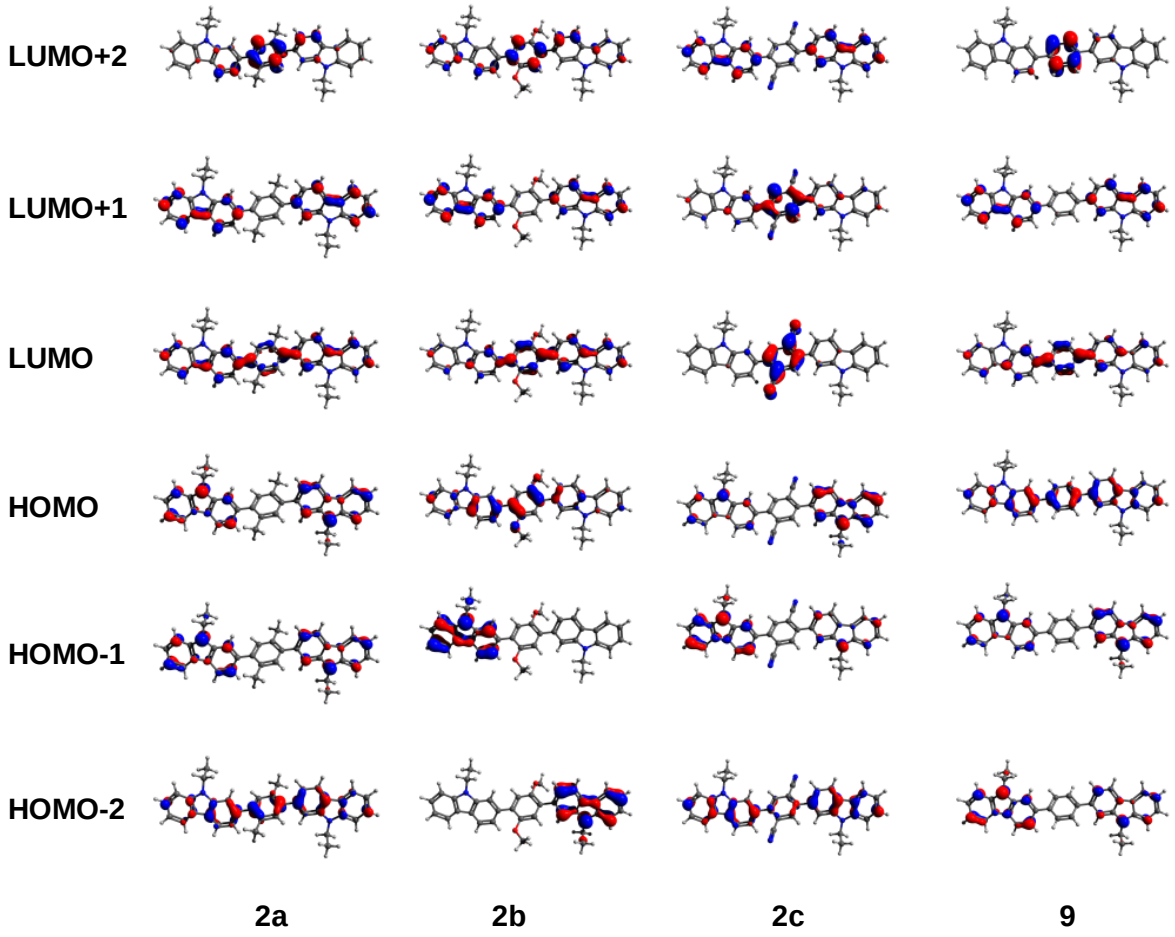

Figure S5 Frontier molecular orbital plots for the complete 2-substituted *N*-ethylcarbazolyl series **2a**–**c** and model compound **9**.

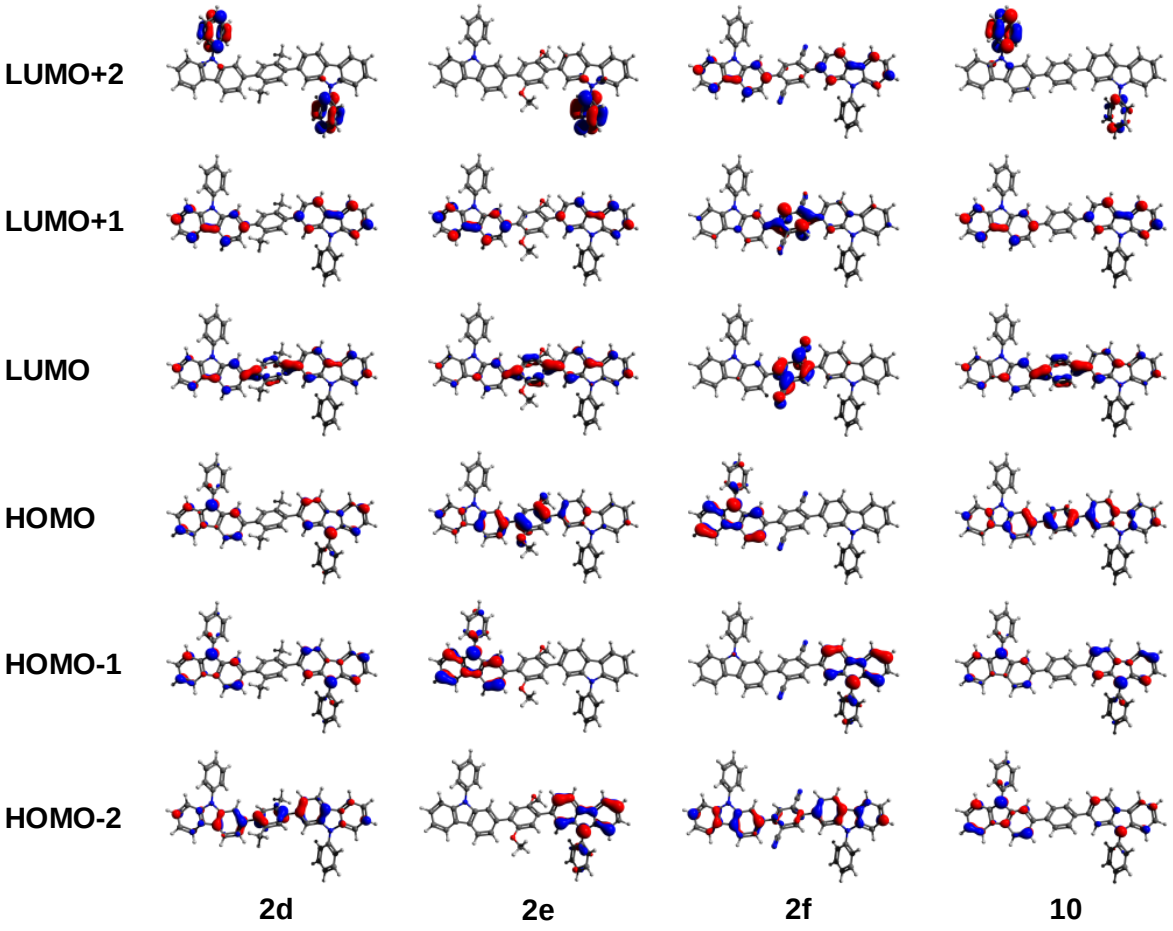

Figure S6 Frontier molecular orbital plots for the complete 3-substituted *N*-phenylcarbazolyl series **2d**−**f** and **10**.

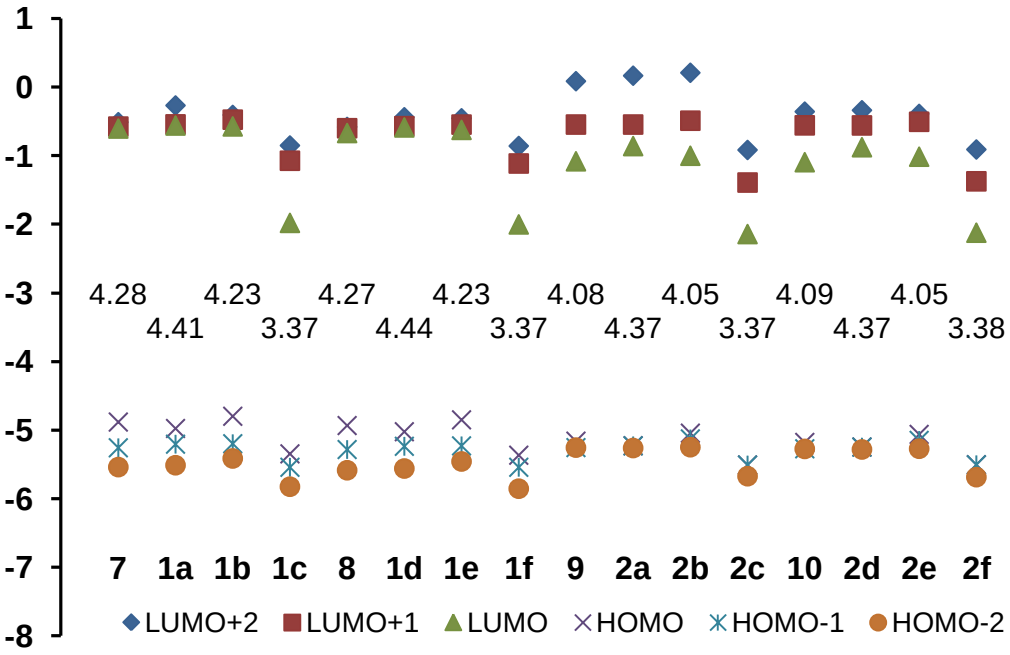

Figure S7 Calculated frontier orbital arrangements of compounds **1a-f** and **2a-f** highlighting the degeneracy in the LUMO manifold of series 1 and the HOMO manifold of series 2.

OLED Devices

Organic light emitting diode (OLED) devices were fabricated on cleaned indium tin oxide (ITO)-coated glass substrates of thickness 125 nm and possessing a sheet resistance of 20 Ω /square. Devices were prepared with the structure: ITO/ NBP (40 nm)/TAPC(10 nm)/18% FIrpic in CBP or in **2d** host(35 nm)/ TAZ(10 nm)/ TPBi(40 nm)/ LiF(0.8 nm)/ Al (100 nm) by thermal evaporation under a vacuum at a pressure of ca. $1x10^{-6}$ Torr. The emissive layer of FIrpic doped into CBP or **2d** was evaporated at a rate of < 1 Å/s, followed by 10 nm of TAZ as a hole blocking layer and 40 nm of TPBi as an electron injection and transport layer, then a deposition of a cathode which consist of a thin layer of 0.8 nm of LiF at a rate of < 0.1 Å/s, capped by a 100 nm layer of aluminium at a rate of 1 Å/s. All samples are encapsulated inside a glove box using DELO UV cured epoxy (KATIOBOND) and capped with 1.2x1.2 cm microscope glass slides then exposed to UV light for 3 min. NBP = *N*,*N*′-di(1-naphthyl)-*N*,*N*′-diphenyl-(1,1′-biphenyl)-4,4′-diamine; TAPC = (1,1-bis{4-*N*,*N*-di(*p*-tolyl)amino]phenyl}cyclohexane); FIrpic = iridium(III) bis[4,6-(di-fluorophenyl)pyridinato-*N*,*C* 2′]picolinate; TAZ = 3-(biphenyl-4-yl)-5-(4-*tert*-butylphenyl)-4-phenyl-4*H*-1,2,4-triazole; TPBi = 2,2′,2″-(1,3,5-benzenetriyl)tris-[1-phenyl-1*H*-benzimidazole].

The current-voltage (*I*-*V*) characteristics and the devices' emission characteristics were measured using a calibrated integrating sphere and the data acquisition was controlled using a home-written NI LabView program which controlled an Agilent Technologies 6632B power supply. The electroluminescence (EL) spectra were measured using a calibrated Ocean Optics USB 4000 CCD spectrometer supplied with 400 µm UV/Vis fiber optic.

References for SI

1. G. M. Sheldrick, *Acta Crystallogr. Sect. A Found. Crystallogr.*, 2008, **64**, 112–122.
2. G. M. Sheldrick, *Acta Crystallogr. Sect. C*, 2015, **71**, 3–8.
3. O. V. Dolomanov, L. J. Bourhis, R. J. Gildea, J. A. K. Howard and H. Puschmann, *J. Appl. Crystallogr.*, 2009, **42**, 339–341.